Mathematical Modelling of Bone Mineralization Integrating Physicochemical Dynamics with Biological Components

Borys Ivan Ostapienko

Department of Biomedical Engineering

Faculty of Medicine

McGill University, Montreal

July, 2018

A thesis submitted to McGill University in partial fulfillment of the requirements of the degree of Master of Biomedical Engineering

Table of Contents

Abstract

Bone mineralization is a critical molecular mechanism of bone remodelling that deposits minerals onto the organic matrix of bone. In the tightly-coupled process, osteoclasts degrade the inorganic matrix by increasing H^+ ions in the bone extracellular matrix, and osteoblasts form the mineralized tissue by controlling the local balance of Ca^{2+} and PO_4^{3-} ion. The process of precipitating hydroxyapatite (HaP) mineral and the mechanisms of its regulation within bone are not yet fully understood; however, cellular, extracellular, and physicochemical events play a role in the remodelling process. The goal of this study was to investigate how the specific role of physicochemical dynamics functions in determining the local balance of Ca^{2+}, PO_4^{3-}, and other minerals. To achieve this goal, I implemented mathematical modelling as a tool to study the HaP precipitation and to explore the mechanisms of defective bone mineralization.

To properly model the precipitation process during bone mineralization, I first examined pertinent literature by performing the scoping review of previously published mathematical models of calcification in biologically-relevant systems. After searching MathSciNet, Scopus, and WebofScience, I screened 2096 studies, and included 114 studies in the final analysis. This scoping review suggested that broad theories, such as classical nucleation and kinetic theories, may be adapted for modelling calcium precipitation in biologically relevant systems; however, detailed mathematical descriptions of biological, chemical, and physicochemical aspects of calcium precipitation are required, but was often missing in published manuscripts.

Next, I developed a mathematical model that combined the description of a) biological regulation of collagen matrix formation and maturation, and turnover of inhibitors of mineralization; b) balance of chemical species related to calcium and phosphate in the aqueous extracellular environment; and c) the precipitation of HaP with biological components through a diffusion-reaction process. The physiological range of initial serum concentrations for Ca^{2+}, PO_4^{3-}, and H^+ that modelled healthy bone mineralization were established. Next, the changes in initial serum concentrations of Ca^{2+}, PO_4^{3-}, and H^+ and their effects on mineral degree formation were investigated. It was determined that Ca^{2+} had the strongest influence on mineral formation. Hypo-mineralization was seen in low concentrations of Ca^{2+} and PO_4^{3-}, consistent with pathological mineralization conditions of hypo-calcemia and phosphatemia. Contrarily, hyper-

mineralization was observed in high concentrations of Ca^{2+} and PO_4^{3-}. Lastly, acidosis causes mineral dissolution and alkalosis promotes mineral formation.

The mathematical model provides an updated outlook on the physicochemical dynamics of bone mineralization. With the addition of aqueous phase species, chemical mineral formation, and the integration with biological components, precipitation dynamics of healthy and defective bone mineralization were studied with changes in specie concentrations in the local bone microenvironment. The outcome of these studies can be used to quantitatively predict mineralization in other tissues and provide insight on the precipitation process of other biological systems.

Key Words: Bone, Modelling, Nucleation, Growth, Calcium, Precipitate

Résumé

La minéralisation osseuse est un mécanisme moléculaire critique du remodelage osseux qui dépose des minéraux sur la matrice organique de l'os. Dans le processus étroitement couplé, les ostéoclastes dégradent la matrice inorganique en augmentant les ions H^+ dans la matrice extracellulaire de l'os, et les ostéoblastes forment le tissu minéralisé en contrôlant l'équilibre local des ions Ca^{2+} et PO_4^{3-}. Le processus de précipitation de l'hydroxyapatite (HaP) minéral et les mécanismes de sa régulation dans l'os ne sont pas encore totalement compris; cependant, les événements cellulaires, extracellulaires et physicochimiques jouent un rôle dans le processus de remodelage. Le but de cette étude était d'étudier comment le rôle spécifique de la dynamique physicochimique fonctionne dans la détermination de l'équilibre local de Ca^{2+}, PO_4^{3-}, et d'autres minéraux. Pour atteindre cet objectif, j'ai implémenté la modélisation mathématique comme outil pour étudier la précipitation de HaP et explorer les mécanismes de minéralisation osseuse défectueuse.

Pour modéliser correctement le processus de précipitation au cours de la minéralisation osseuse, j'ai d'abord examiné la littérature pertinente en effectuant l'examen de la portée des modèles mathématiques de calcification publiés antérieurement dans des systèmes biologiquement pertinents. Après une recherche sur MathSciNet, Scopus et WebofScience, nous avons analysé 2096 études et inclus 114 études dans l'analyse finale. Cette revue de la portée suggérait que de larges théories, telles que les théories classiques de nucléation et de cinétique, pourraient être adaptées pour modéliser la précipitation du calcium dans des systèmes biologiquement pertinents; cependant, des descriptions mathématiques détaillées des aspects biologiques, chimiques et physicochimiques de la précipitation du calcium sont requises, mais elles manquaient souvent dans les manuscrits publiés.

Ensuite, j'ai développé un modèle mathématique qui combine la description de a) la régulation biologique de la formation et de la maturation de la matrice de collagène, et le renouvellement des inhibiteurs de la minéralisation; b) l'équilibre des espèces chimiques liées au calcium et au phosphate dans l'environnement extracellulaire aqueux; et c) la précipitation de HaP avec des composants biologiques par un processus de diffusion-réaction. La gamme physiologique des concentrations sériques initiales de Ca^{2+}, PO_4^{3-} et H^+ qui ont modélisé la minéralisation osseuse saine ont été établies. Ensuite, les changements dans les concentrations sériques initiales 8 de

Ca^{2+}, PO_4^{3-} et H^+ et leurs effets sur la formation du degré minéral ont été étudiés. Il a été déterminé que Ca^{2+} avait l'influx le plus fort sur la formation minérale. Une hypominéralisation a été observée à de faibles concentrations de Ca^{2+} et de PO_4^{3-}, ce qui est compatible avec les conditions de minéralisation pathologique de l'hypocalcémie et de la phosphatémie. Au contraire, une hyperminéralisation a été observée à de fortes concentrations de Ca^{2+} et PO_4^{3-}. Enfin, l'acidose provoque la dissolution des minéraux et l'alcalose favorise la formation de minéraux.

Le modèle mathématique fournit une perspective actualisée sur la dynamique physicochimique de la minéralisation osseuse. Avec l'ajout d'espèces en phase aqueuse, la formation de minéraux chimiques et l'intégration avec des composants biologiques, la dynamique des précipitations de minéralisation osseuse saine et défectueuse a été étudiée avec des changements dans les concentrations d'espèces dans le microenvironnement osseux local. Les résultats de ces études peuvent être utilisés pour prédire quantitativement la minéralisation dans d'autres tissus et fournir un aperçu du processus de précipitation d'autres systèmes biologiques.

Abbreviations

ACP – Amorphous calcium phosphate

CNT – Classical Nucleation Theory

CP – Calcium precipitate

CPP – Calcium phosphate precipitates

DCPD – Dicalcium phosphate dihydrate

ECM – Extracellular matrix

HaP – Hydroxyapatite

MCaT – Initial serum concentration of calcium

MHT – Initial serum concentration of hydrogen

MPO4T – Initial serum concentration of phosphate

OCP – Octacalcium phosphate

RANK – Receptor activator of nucleator factor kB

RANKL – Receptor activator of nucleator factor kB-ligand

TCP –Tricalcium phosphate

List of Tables

List of Figures

Contribution of authors

To adhere to the standards set out by the Faculty of Graduate and Postdoctoral Studies of McGill University, the contribution of all authors for each chapter included in this thesis is listed below. All chapters included in this thesis were written by Borys Ivan Ostapienko and revised by Dr. Svetlana V. Komarova.

Chapter 1: Borys Ivan Ostapienko collected the background information necessary to explain the process of bone remodelling. Dr. Svetlana V. Komarova provided suggestions for editorial revisions.

Chapter 2: Borys Ivan Ostapienko collected, reviewed, and categorized, all studies included in the scoping review, with feedback on number and type of categories from Dr. Svetlana V. Komarova. April Colosimo, the library liaison for the department of biomedical engineering, formulated the search strategy and keywords associated for the scoping review. Domenico Lopez acted as the second individual reviewer for the scoping review, which involved screening the articles and consulting on discrepancies found. Detailed analysis into the theories for calcium precipitation was conducted by Borys Ivan Ostapienko, with extensive feedback and revisions from Dr. Svetlana V. Komarova.

Chapter 3: Borys Ivan Ostapienko developed the MatLab code for the updated mathematical model and performed computer simulations and testing to obtain the results. Volumetric constraints for mineral formation were suggested by Dr. Svetlana V. Komarova and implemented into the MatLab code by Borys Ivan Ostapienko.

Chapter 4: Borys Ivan Ostapienko conducted a detailed analysis of the work presented and concluded the findings found with the revision and editing of Dr. Svetlana V. Komarova.

Acknowledgements

I would like to express my sincerest thanks to my supervisor Dr. SV Komarova for her invaluable guidance, and for always inspiring me to think outside the box, leading to new ideas and critically progressing throughout my research.

I would also like to thank the liaison librarian, April Colosimo, who was able to give an external outlook on my research, which helped guide the beginning stages of my research.

Special thanks go out to my lab mate, Domenico Lopez, who so favourably agreed to be a secondary peer reviewer in the literature review portion of my research.

I would like to express my deepest appreciation to Dr. Gula, Dr. Kerstein, Dr. Iris Boraschi, and Nicholas Mickolajewicz, for familiarizing me with the specialized techniques used in cell culture towards bone research and for guiding my research in the wet-lab.

I am also grateful for all of my lab mates, especially Turney Mckee and Mariya Stavnichuk, who always found a way to bring joy into everyday of the week.

I would like to thank the funding agencies of NSERC and CIHR that have made this research possible, which continue to support Canadian research and innovation for the better.

Thank you to all my friends, new and old, that have supported me throughout this journey and the many memories that I will cherish.

A final thank you goes out to my parents, for their endless support, continuous encouragement, and years of dedication throughout my years of study and the process of my thesis research studies.

Introduction

Biomineralization is the process by which minerals are incorporated into biological tissues to provide structural support and enhance mechanical integrity of the tissue. In human bones, these minerals consist of calcium and phosphate to produce calcium salts, specifically hydroxyapatite (HaP), that together with organic components, such as collagen, form a composite material of bone.

During the process of bone remodelling, osteoblasts produce organic matrix and regulate the availability of calcium and phosphate, which facilitates the formation of HaP crystals within the the organic matrix. The formation of HaP at specific locations in the organic matrix is a complex process that requires the involvement of several proteins that are present within the extracellular space of the bone microenvironment. Nucleator proteins are required to promote the precipitation of HaP onto the organic matrix; however, inhibitors are also present to prevent immature organic matrix from mineralization. Therefore, it is important to understand the biologically regulated precipitation of calcium phosphate in human bone in order to explain the biomechanical function and develop a biomimetic construct of the system.

Calcium precipitation from solution consists of two general phases: 1) crystal nucleation encompassing the formation of microcrystalline units that later act as centers of crystallization and 2) crystal growth resulting in formation of macro-crystals. Nucleation of calcium precipitate (CP) can occur spontaneously (homogenous nucleation) or can be induced by the presence of foreign particles or impurities in the system (heterogeneous nucleation). In biological systems, proteins commonly act as the foreign particles initiating the nucleation process (Wang et al., 2008). Once the CPs are nucleated, crystal growth occurs in a surface-controlled manner, only to be limited by inhibitors present on the nucleating surface. Crystal formation depends on a number of parameters, including ion concentration, acidity (pH), and temperature (Lu & Leng, 2005; Oliveira, Ferreira, & Rocha, 2007). In the biological microenvironment many of these parameters are controlled, providing additional constrains on the formation. For example, formation of calcium phosphate precipitates (CPP, the most physiologically relevant CP) depends on the concentrations of hydroxide (OH^-) and phosphate (PO_4^{3-}), which in turn are controlled by the body depend on an associated bicarbonate and phosphate buffering system, together stabilizing the value of the pH in the system (Mohan, 2006). These processes are

strongly interdependent, so that changes in one component (hydroxide or phosphate), will lead to non-linear changes in the other components. Similarly, temperature critically affects growth of CPs by modifying the thermodynamic favourability of precipitation-dissolution reaction described by the solubility constant (K_{sp}). This causes critical changes in the dynamic equilibrium of ion exchange between solute and solution, modifying the crystal growth kinetics (Rice, Barber, O'Connor, Stevens, & Kentish, 2010). Thus, the presence of a biologically-rich microenvironment critically affects the already physicochemically complex process of CP crystallization.

Theoretical work aimed at understanding phase transitions during crystallization, condensation, boiling and melting, all of which are characterized by nucleation and growth, goes back to as early as the 19th century (Kalikmanov, 2013). While significant progress was made, such as the development of classical nucleation theory (CNT) (Gibbs, 1878; Volmer, 1926), surface kinetic energy and diffusion theories of crystal growth (Gibbs, 1878; Noyes & Whitney, 1897), this work is still ongoing, in particular with respect to understanding the molecular level events occurring during nucleation and growth (Karthika, Radhakrishnan, & Kalaichelvi, 2016). The classical approaches to describe physicochemical aspects of CP formation were used to model the calcification in biological fluids (Lu & Leng, 2005; Wang et al., 2012; Xie, Liu, Chu, & Ding, 2006); however, taking into account more complex biological components required the development of more original approaches to account for the contribution of physicochemical and biological factors (Barat, Montoya, Seco, & Ferrer, 2011; Petersson et al., 2004).

Few attempts were made to develop mathematical models of biologically-controlled mineralization occuring in bone and teeth (Komarova et al., 2015; Martin, 1994). It is evident, that developing mathematical models that consider both biological and physicochemical controls of mineral formation is challenging, due to the conceptual and computational complexity of such models. As the regulation of extracellular signalling between proteins, cells, and matrices towards HaP precipitation is not clearly understood in bone mineralization, a mathematical model linking physicochemical kinetics with the biology of bone was developed. The mathematical model investigated the formation dynamics of HaP mineral and its associated molecular and cellular interactions with the biological processes of bone formation. Knowing the underlying mechanisms of bone mineral formation can potentially lead to predicting pathological

mineral disease states (such as hyper/hypo-calcemia and –phosphatemia), with the capability of understanding mineralization disorders of unknown etiology (Komarova et al., 2015).

Rationale and Hypothesis

It is apparent that bone mineralization involves biological and physicochemical processes that aid in the formation of the inorganic matrix. The mechanisms by which these processes occur are yet to be fully understood as the extent of biological and chemical coupling from osteoblasts and the surrounding extracellular environment are unknown. As bone mineralization is determined to be a tightly regulated and nonlinear process, mathematical modelling is capable of predicting these dynamics and providing further insight into the local balance of minerals and its effect on mineral formation. The primary objective of this work was to characterize the contribution of physicochemical precipitation mechanism during bone mineralization.

First, I performed the scoping literature review of mathematical modelling approaches used to describe calcium precipitation in biological systems. The goal of this scoping review was to provide an overview of existing mathematical models describing the formation of calcium precipitates in biological systems and identify potential gaps and limitations. For the most widely used approaches, additional analysis was provided with respect to their ability to describe physicochemical aspects of crystal formation in the biological environment. This study resulted in a manuscript *BI Ostapienko, D Lopez, and SV Komarova (2018) Mathematical modelling approaches to study calcification in biological systems: scoping review*, currently in revision in the journal *Biomechanics and Modeling in Mechanobiology*.

Second, I developed a mathematical model that described physicochemical dynamics of related ions in extracellular fluid, their precipitation, as well as changes in biological components present during bone mineralization. The goal of this study was to investigate how changes in serum concentrations of Ca^{2+}, PO_4^{3-}, and H^+ affect the formation of HaP mineral in physiological and pathological ranges of concentrations, and to compare to bone mineral disease states observed in hypo- and hyper-phosphatemia and calcemia. Chapter 3 represents a draft of the manuscript to be submitted.

Chapter 1: Anatomy and Physiology of Bone

1.1 Structure and Composition of Bone

Despite bone being inert in appearance, mineralized connective tissue found in bone is highly dynamic with a range of functions (Florencio-Silva, Sasso, Sasso-Cerri, Simões, & Cerri, 2015). These functions include supporting and protecting soft tissues, interacting with muscles for locomotion, housing the process of hematopoiesis, and storage of calcium and phosphate, amongst other vitamins and minerals (Robling, Castillo, & Turner, 2006). There are three major cells that contribute to the bones structure, osteoblasts, osteoclasts, and osteocytes, which work together to form the organic and inorganic components of bone.

1.1.1 Bone Cells (Osteoblasts, Osteoclasts, and Osteocytes)

Osteoblasts are bone forming cells that synthesizes new bone by secreting the organic matrix and depositing mineral onto the organic matrix (Siddiqui & Partridge, 2016). Collagenous proteins, primarily consisting of type-I collagen, make up the majority of the organic matrix. Matrix mineralization, in osteoblasts, occurs when matrix vesicles are released into the bone matrix and bind to the mature organic matrix (Anderson, 2003). They also act as storage for minerals involved in precipitation, maintaining the pH (hydrogen-ion activity) and ion concentration balance (Yoshiko, Candeliere, Maeda, & Aubin, 2007).

Osteoclasts are bone abolishing cells that resorb bone by creating an acidic microenvironment to dissolve the mineral component of bone (Florencio-Silva et al., 2015). These bone resorbing cells are activated by RANKL (receptor activator of nucleator factor kb ligand) and MCS-F (macrophage colony-stimulating factor), both of which are produced by neighbouring osteoblast cells. The secretion of cathepsin K enzyme and hydrogen ions by osteoclasts dissolves the proteinaceous matrix and inorganic mineral, respectively. Osteoprotegerin (OPG), produced by osteoblasts, binds to RANKL, preventing binding to RANK on the osteoclast (Boyce & Xing, 2008).

Osteocytes are cells located within the lacunae of bone that were once osteoblasts secreting within the matrix but became trapped (Schaffler, Cheung, Majeska, & Kennedy, 2014).

Osteocytes interact with the other bone cells through mechanosensory mechanisms that send signals of resorption or formation of bone (Florencio-Silva et al., 2015).

1.1.2 Bone Metabolism

Bone metabolism consists of the constant modelling and remodelling process, where bones adapt in response to a physiologic influence or mechanical force (Clarke, 2008), as well as changes in systemic factors including hormones, cytokines, and chemokines (Raisz & Rodan, 1998). Bone modelling is mostly associated with the overall shape of bone changing through osteoblast or osteoclast recruitment in response to a biomechanical force, where formation and resorption are not tightly coupled (Clarke, 2008). Although this process is not uncommon, bone remodelling occurs more frequently and is a continuous process that spans the lifetime of an individual (Kobayashi et al., 2003).

Figure 1: Four distinct steps of the bone remodelling process (Kapinas & Delany, 2011).

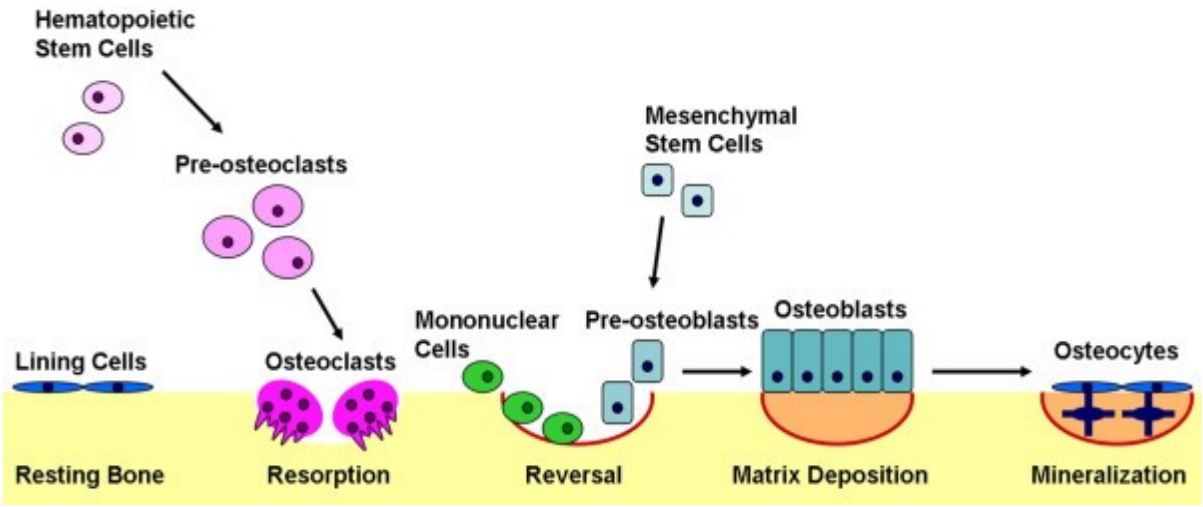

Bone remodelling is the continuous process where old bone is replaced with new bone to maintain bone strength and mineral homeostasis (Dallas, Prideaux, & Bonewald, 2013). Bone resorbing osteoclasts remove the old bone while bone forming osteoblasts lay down and mineralize the organic matrix to form new bone. This tightly coupled process occurs in four distinct steps (***Figure 1***): 1) activation, where mononuclear monocyte-macrophage osteoclast precursors are recruited and activated to form pre-osteoclasts that interact with osteoclasts

(Roodman, 1999), 2) resorption, where osteoclasts increase acidity and secrete proteases to degrade the bone mineral and organic matrix (Silver, Murrills, & Etherington, 1988), 3) reversal, where osteoclast resorption decreases and pre-osteoblasts are signalled by bone matrix-derived factors to begin bone formation (Locklin, Oreffo, & Triffitt, 1999), and 4) formation, where osteoblasts synthesize newly formed organic matrix and mineralize the matrix. Quiescence occurs once bone formation has been completed and osteoblasts become dormant (bone lining cells) on the bone surface. The tightly-coupled process between osteoclasts and osteoblasts that arranges the organic matrix (and its mineralization) is critical in determining the mechanical integrity of the newly formed bone.

1.2 Organic Bone Matrix

The organic bone matrix is deposited by osteoblasts and mainly consists of collagenous proteins produced within the extracellular matrix (ECM), primarily composed of type-I collagen, with non-collagenous proteins completing the composition (Florencio-Silva et al., 2015). Within the bone extracellular microenvironment are inhibitor and nucleator molecules that regulate mineralization.

1.2.1 Collagen Matrix

The secretion of organic matrix is initiated by osteoblasts and deposits the naïve organic matrix (***Figure 2***). To allow mineralization on the organic matrix, the naïve matrix must go through the process of matrix maturation. During maturation, key post-translational modifications, such as the cleavage of C- and N-terminal propeptides from collagen and crosslinking of collagen, occur in the ECM to allow naïve matrix maturation (Knott & Bailey, 1998). Collagen crosslinking and peptide synthesis from collagen affects the mineralization process and the mechanical properties, specifically tensile strength of bone, due to the arrangement of collagen fibers (Garnero, 2012). During matrix maturation, inhibitor molecules are present to control the mineralization process.

1.2.2 Inhibitors & Nucleators

Inhibitor molecules, such as inorganic pyrophosphate, are present in the local bone extracellular microenvironment to prevent the mineralization of the naïve matrix (D. & Antonio, 1996; Murshed & McKee, 2010). Inhibitor molecules include proteins and minerals, some of which are:

SIBLING protein family, osteopontin, osteocalcin, sclerostin, bone morphogenic proteins, inorganic pyrophosphate, and magnesium (Margolis, Kwak, & Yamazaki, 2014). These inhibitor molecules affect the mineralization in solution and on collagen surfaces depending on the characteristics (structure, shape, and function) of the inhibitor. For example, sclerostin acts through the regulation of the PHEX/MEPE signalling pathway in solution, which inhibits the proliferation of osteoblasts and maturation of chondrocytes (Atkins et al., 2012). The inhibition efficacy of pyrophosphate in solution depends on the number of hydrolyzed phosphate molecules, where hydrolysis of pyrophosphate yields two orthophosphate molecules to remove the inhibitory activity (Meyer & Reddi, 1985). Osteocalcin and osteopontin behave as inhibitors in solution by binding to specific faces of the mineral crystal; however, osteocalcin can also become a nucleator when bound to collagen, where it interacts with different faces of the mineral crystal (Chen, Jacquet, Lowder, & Landis, 2014). Inhibitor molecules prevent matrix mineralization by competing with the inorganic mineral (HaP) to deplete ion binding or by protein adsorption on the naïve matrix (Palmer, Newcomb, Kaltz, Spoerke, & Stupp, 2008).

The inhibitor molecules are eventually degraded by isozymes (Sebastián-Serrano et al., 2015) and enzymes to permit mineralization. Once inhibitors are degraded within the local bone extracellular bone microenvironment, nucleators promote and guide the process of mineral crystal formation. Nucleator molecules, such as bone sialoprotein and dentin matrix protein 1, have a high affinity for calcium ions (Oldberg, Franzen, & Heinegard, 1988), that guide the individual crystals between or within the collagen fibrils (interfibrillar and intrafibrillar mineralization, respectively). Bone sialoprotein also contains chains of salicylic acid, which allow the protein to tightly bind to the alpha-2 chain of interfibrillar collagen. This nucleation process, driven mainly by chemistry and matured matrix, initiates mineral precipitation, where the inorganic bone matrix begins to form.

Figure 2: Organic extracellular matrix and inorganic matrix components of bone mineralization (Mescher, 2016).

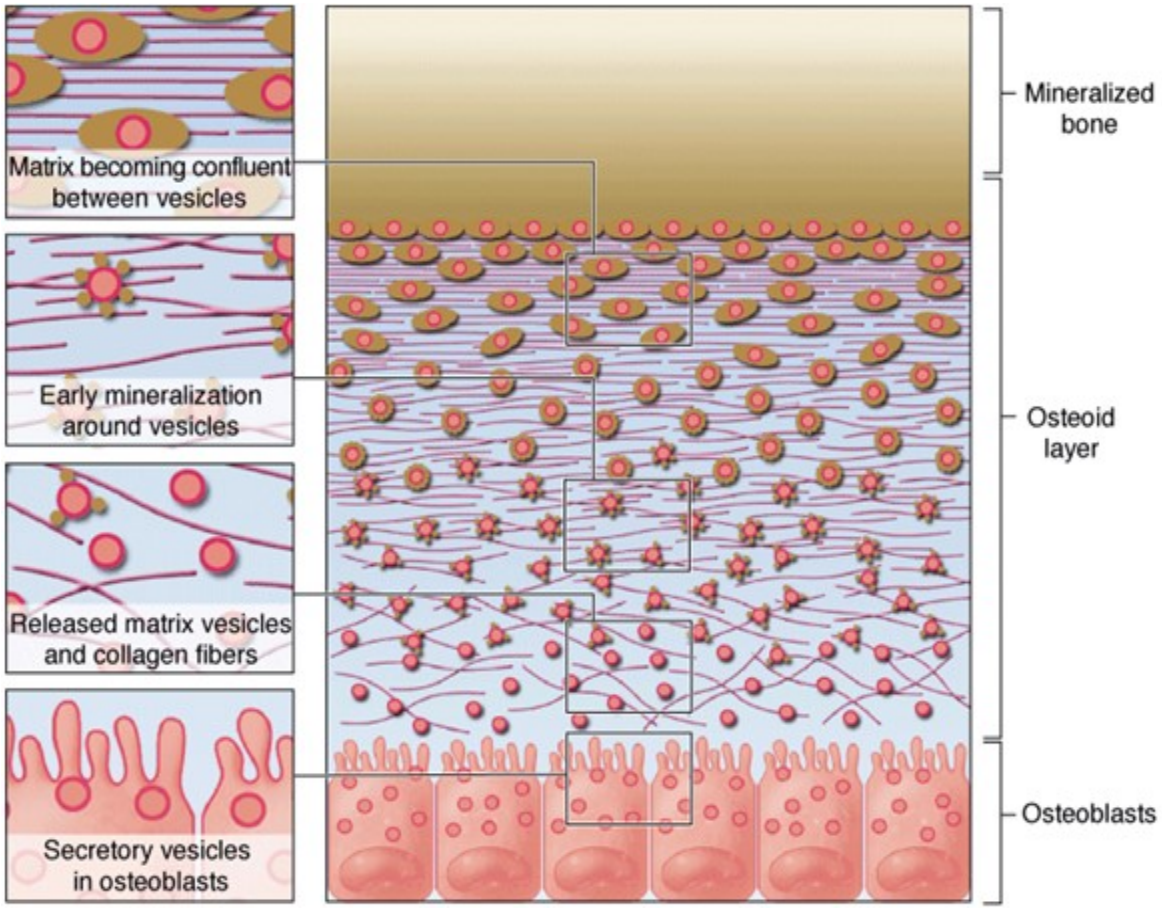

1.3 Inorganic Bone Matrix

The outer layer of bone tissue predominately consists of calcium and phosphate ions; however, other chemical elements, such as bicarbonate, are also present. These chemical elements react in a series of chemically-driven reactions influenced by biological inhibitors and catalysts to form the hard inorganic mineral of bone – HaP. The mineral content of bone is responsible for providing strength and support at times of mechanical resistance.

1.3.1 Mineral Formation

Chemical elements present in the local bone microenvironment bind to nucleators present on the mature organic matrix to initiate the mineralization process. The organization of these crystals is dependent on the concentrations of these chemical elements, as well as the concentration and

localization of nucleators within or on the mature organic matrix. Matrix extracellular vesicles contain the necessary concentrations of chemical elements to precipitate HaP crystals, inducing a locally saturated state where HaP crystals are promoted to nucleate and grow (Anderson, 2003). As the last stage of bone formation continues, HaP crystals enlarge due to the constant supply of chemical elements to the sites of nucleation until equilibrium between the ECM and site of mineralization is reached. Nucleator molecules and macromolecules may also bind to the initial crystal to facilitate the orientation and geometry of crystals formed (Clarke, 2008).

1.3.2 Pathological Mineral Formation

The concentration of inhibitors, nucleators, and chemical elements, as well as the structure and orientation of collagen fibrils within the organic matrix, affects the balance of bone homeostasis. An imbalance between the bone resorption and bone formation may lead to hyper- or hypo-mineralized states of mineralization, which can later become bone mineralization diseases. Osteomalacia and rickets are bone mineralization diseases that occur due to decreased levels of vitamin D in the body (Reuss-Borst, 2014). With low levels of vitamin D in the body, calcium availability for precipitating HaP in bone is reduced, leading to weak and soft bones due to reduced bone strength, hardness, and fracture toughness. Osteogenesis imperfecta VI can be similarly characterized by brittle bones due to mineralization defects, even though the genetic defect is currently unknown (Glorieux et al., 2002). These bone mineralization diseases are the result of changes in mineral impurity production of HaP mineral, eventually leading to the compromised mechanical integrity of the bone (Appelman-Dijkstra & Papapoulos, 2015).

Chapter 2: Mathematical Modelling of Calcium Phosphate Precipitation in Biologically Relevant Systems

2.1 Introduction

Although the organizational location of hydroxyapatite crystals on collagen has been well established, the mechanism by which mineral precipitates within bone is largely still unknown. By investigating other biologically-relevant systems that precipitate calcium phosphate-derived minerals, the studies of the mechanisms by which mineral precipitation occurs in bone could be informed. Developing mathematical models that take into account both biological and physicochemical controls of mineral formation is difficult, due to the conceptual and computational complexity of such models. Therefore, I performed a scoping literature review aimed to provide an overview of existing mathematical models describing the formation of calcium precipitates in biological systems. Additional objectives included identifying potential gaps and limitations in the current literature and providing additional analysis of the most widely used approaches to evaluate their ability to describe physicochemical aspects of crystal formation in the biological environment.

2.2 Methods

Eligibility criteria: I aimed to include the full-length manuscripts describing mathematical models of calcification in biological systems. No limit for year or language of publication was introduced. Conference abstracts and general books on the topic were excluded, however full-length conference proceedings and book chapter's specifically describing mathematical modelling approaches were included.

Information sources: The search was performed on November 30th, 2017, in three databases, MathSciNet, Scopus, and WebofScience. References and citations of selected manuscripts were perused, but did not provide additional sources.

Search: The search strategy was built with the assistance of the McGill librarian, and included the following keywords and their derivatives searched for in article title, abstract or keywords: model, expression, nucleation, calcium, precipitation, mineral, growth, and phase transformation. The full search for Scopus was: (nucleation OR nucleus OR nuclei) AND (Model* OR

expression* OR equation* OR math* OR computat*) AND (Calcium) AND (Precipitat* OR mineraliz* OR biomineraliz*) AND (grow OR grows OR growth OR Phase transformation). Biological application was not specified in the search to increase sensitivity, however in MathSciNet the biological/medical models were pre-selected within the search engine.

Study selection: Data was extracted from the databases to Endnote reference management software, where the duplicates were removed. The resulting library was uploaded to Rayyan QCRI, the Systematic Reviews web app (https://rayyan.qcri.org) (Ouzzani, Hammady, Fedorowicz, & Elmagarmid, 2016), where additional duplicates were identified and removed, and selection was independently performed by two co-authors (BIO and DL), who assessed study eligibility based on: title, abstract and provided key terms. In case of disagreement the papers were discussed and included based on consensus. The included papers were those that applied mathematical modelling (consisting of equations in some form) to calcium precipitation in a biological system (part or a whole, interaction with, or representation of any living entity). Following abstract/title/keyword screening, the full text of selected papers was assessed to confirm their eligibility.

Data collection process: All eligible papers were classified using the full text for the following categories:

1) Biological system: unlimited number of categories summarizing biological systems directly studied or stated as directly applicable to the model. Information regarding modelling biological aspects of the process was also extracted.

2) Calcium precipitate being studied: unlimited number of categories

3) Calcification process that was being modeled, with four categories: nucleation, growth, crystallization process, and metastable-state phase transformation.

4) Level of generalization, separated into three categories: general (applicable to a wide range of biological systems), bioprocess (a model that could be applied to a specific subset of a biological system, i.e. wastewater), and tailored (a specific biological process was studied).

5) Theory, separated into three categories: classical nucleation theory (CNT) and kinetic approach, and the third category comprising of theories not directly derived from CNT or kinetic theory.

2.3 Overview of Papers Modelling CPs

The electronic search for manuscripts describing mathematical models of CP formation in biological systems returned a total of 2096 unique articles, 413 of which were identified as potentially relevant after title/abstract screening. After the full text screening, 114 articles were included in the final qualitative study (***Figure 3A***). The first papers describing modelling of biologically relevant calcification appeared in the 1980s, after which the interest in this topic steadily increased (***Figure 3B***).

Figure 3: A. Flow chart of articles through the scoping review process B. Number of publications on the topic of calcium phosphate precipitation per year

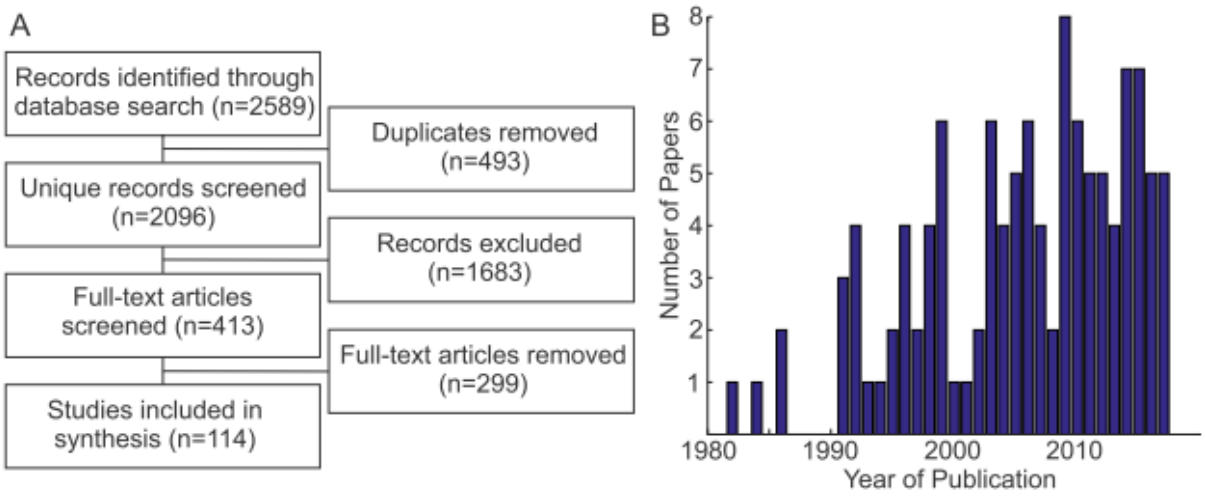

2.3.1 Investigated Biological Systems

The mathematical models developed to date aimed to understand diverse systems where biology overlaps with physical chemistry of calcium precipitation (***Figure 4A***). The largest number of studies (48/114) was focused on human biological tissues, including physiological calcification of bone (12/48), and regulation of mineral homeostasis (7/48); pathological calcification such as formation of kidney stones (5/48); detailed interactions of proteins with calcified material (9/48); and preparation of tissue engineered bone and dental implant (15/48). Water research systems,

including wastewater treatment and purification was the next most common application (38/114) where biological factors need to be considered to understand formation of calcium precipitates. Agricultural application, such as soil quality (9/114), dairy ultrafiltration (4/114), and geochemical (4/114), as well as geothermal (precipitation in volcanic environment) (9/114), and oilfield (2/114), were the focus of the last third of the manuscripts. Theoretical description of associated biological processes was only performed in 13 of 114 studies, majority of which were focused in human biological tissues (12/114). Thus, the diverse fields of study for calcium precipitation highlighted the importance of this interdisciplinary research field. Information regarding modelling chemical aqueous phase was also extracted.

Figure 4: A. Pie chart characterizing the type of biological system studied – divided into three categories: pink – agricultural sciences, green – human biological tissue, yellow – water systems research. B. Pie chart characterizing the type of calcium phosphate being studied – divided into two categories: Orange – CPPs, Cyan – non-CPPs. [Other[1] includes: calcium fluoride, fluorapatite, dolomite, calcium peroxide, calcium magnesium mix; Other[2] includes: carbonated HaP, calcium pyrophosphate dehydrate, and monocalcium phosphate]

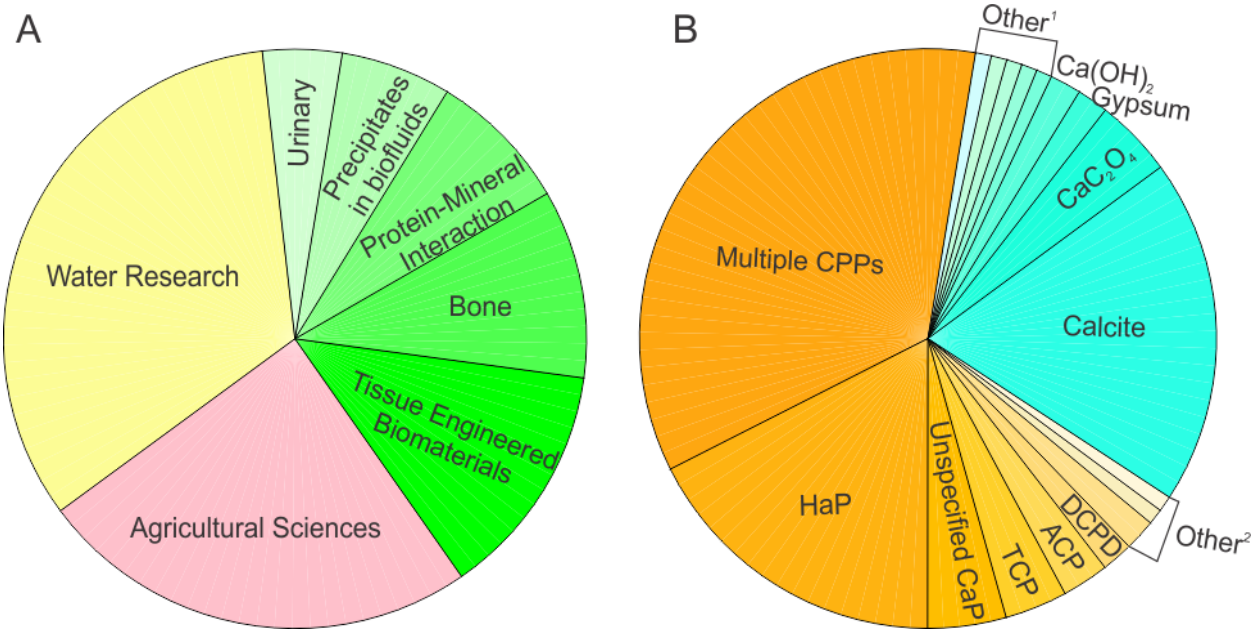

2.3.2 Calcium Precipitates Studied

The developed models studied the formation of multiple types of calcium precipitates (***Figure 4B***). The largest proportion of the articles screened was focused on understanding the formation of calcium phosphates (78/114), followed by calcium carbonate (22/114), and more unique calcium salts. Precipitation of calcium phosphate was studied since it is particularly important for human biological systems, and is the most common precipitate formed in wastewater or soil. Calcium carbonate (22/114) and oxalate (5/114) were also mostly studied in their relevance to human biology, (patho)physiology and tissue engineering. One of particularities encountered during theoretical and experimental studies of calcium phosphate precipitation is the occurrence of multiple species of CPPs (***Table 1***). Hydroxyapatite ($Ca_{10}(PO_4)_6OH_2$, HaP) is the most biologically relevant form of CPP. A number of intermediate precursors and metastable states may be formed under specific conditions including: amorphous calcium phosphate, brushite or dicalcium phosphate, tricalcium phosphate, and octacalcium phosphate (Barat et al., 2011; Wang & Nancollas, 2008). Each precipitate has its stoichiometric Ca/P ratio ranging from 1.00 to 1.67; however, in biological systems, these CPP may deviate from ideal Ca/P ratio due to micro-environmental factors and impurities (Wang & Nancollas, 2008). Significant number of studies addressed this aspect of calcium phosphate precipitation (40/114), while 38/114 studies investigated only a single calcium phosphate species.

Table 1: CPPs present in biologically relevant systems

Calcium Phosphate Precipitate	Chemical Formula	Ca/P Ratio	pH[1]	Precipitate Stage Formation	Properties
Amorphous Calcium Phosphate	$Ca_xH_y(PO_4)a\cdot xH_2O$	1.18-2.5	5-11	ACP → ANY[2]	Highly soluble pH-dependent
Dicalcium Phosphate Dihydrate	$CaHPO_4\cdot 2H_2O$	1.0	<6.5	DCPD → OCP	Primary CPP HAP precursor
Tricalcium phosphate	β-$Ca_3(PO_4)_2$	~1.5	5-9	DCPD → β-TCP	Needs Mg^{2+} presence Soluble
Octacalcium phosphate	$Ca_8(HPO_4)_2(PO_4)_4\cdot 5H_2O$	1.3-1.5	6.5-8	DCPD → OCP → HaP	Metastable Low solubility
Hydroxyapatite	$Ca_{10}(PO_4)_6(OH)_2$	1.67	6.8-9	ACP → OCP	Thermodynamically

[1] pH refers to the acidity/alkalinity of the environmental conditions required for precipitate formation to occur

[2] Where ANY is any other calcium phosphate precipitate other than ACP

				→ HaP	favourable Prevalent in biosystems

2.3.3 Theoretical approaches to model calcium precipitation

Next, I characterized theoretical approaches used in the published literature. General models of how biological factors may influence calcification were developed in 32/114 studies. More focused approaches, undertaken in 61/114 studies, described the models developed for specific biological field, but applicable to the related systems (such as soil and water), were classified as bioprocess model types. Models developed to address very specific situations were classified as tailored (21/114) (***Figure 5A***).

Figure 5: Pie charts characterizing the modelling approaches to study biological calcification. A. Type of model used. B. Primary process during CP formation that was modeled. C. Type of theory used.

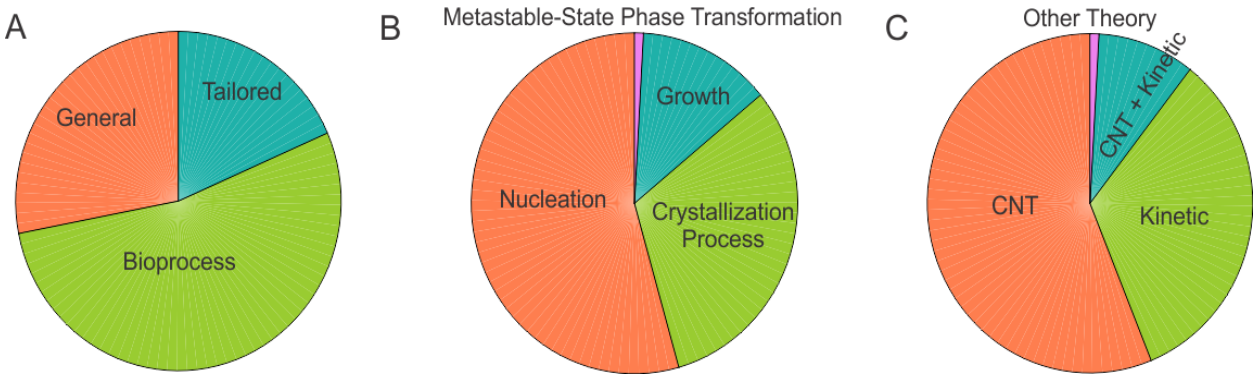

Next I analysed which aspect of the calcification process was the focus of the model (***Figure 5B***). Calcium precipitate formation (or crystallization) is the process by which highly ordered molecules arrange to form the crystal lattice structure, resulting in formation of a crystalline solid material (Wang & Nancollas, 2008). Two simultaneous processes are distinguished during crystallization reactions, crystal nucleation and crystal growth, that occur in the bulk solution and at the interface with the existing solids respectively. Nucleation involves formation of small units that later act as centers of crystallization, with two distinct cases: 1) homogeneous nucleation, when precipitate forms spontaneously, and 2) heterogeneous nucleation, when foreign particles or impurities initiate precipitate formation (De Yoreo, 2003). During the phase of crystal growth, these centers of crystallization or pre-existing crystals expand in size. There are necessary

conditions that need to be met in order for crystallization to transpire: 1) the system must be in a supersaturated state to allow the precipitation in the bulk of the solution, 2) appropriate ion collisions and bond-breakage must surpass the surface energy barrier for formation of critical-sized nuclei, and 3) the continuous growth of highly ordered molecules have to be maintained by ion delivery from supersaturated solution (Wong & Czernuszka, 1993). Nucleation was modeled as the key crystallization event in 62 of 114, with the early theories focusing on nucleation as the primary event of calcium precipitation. While some papers modeled growth as the key crystallization event (15/114), most recent studies took into account both nucleation and growth and were classified as crystal formation (36/114). Finally, a somewhat distinct approach was to model the metastable phase transformations of CPs (1/114) to determine the final proportion of stable crystalline solid formed once nucleators and growth factors are exhausted.

Finally, I aimed to classify and describe the theories used in modelling calcium precipitation of biological systems (***Figure 5C***). During crystallization, the processes of nucleation and growth occur at varying temporal and spatial scales that require different approaches to take them into account. Depending on the researcher's spatial and temporal scale of interest, the mass of solid material being deposited over time within a given system was estimated using different approaches, which take into account thermodynamic, mass transfer or kinetic processes. The majority of papers (64/114) modeled calcium precipitation using thermodynamics-based classical nucleation theory (CNT). Another widely utilized approach was the kinetic theory (38/114). A combination of CNT and kinetic theories was used in (11/114) papers, while one paper described phase transformation in a unique way.

2.4 Crystal Precipitation Theories

2.4.1 Classical Nucleation Theory - Thermodynamic Considerations

When the initialization of crystal formation and the early stages of crystal growth were of interest, thermodynamics needs to be considered in detail. Thermodynamic reasoning is based on understanding the energy requirements for formation of the organized crystal structures in comparison for the energy drive of the supersaturated solution (Gibbs, 1878). The thermodynamic favourability for the precipitate to form was determined by Gibbs thermodynamic free energy change, ΔG, which could be estimated from physicochemical characteristics of the reaction. The rate of nucleation describing the formation of new structures

through self-organization of molecules by thermally-driven processes could be described using the variation of Arrhenius equation (Mullin, 2001).

$$N = Kexp\left(-\frac{\Delta G}{kT_K}\right) \quad (1)$$

Where N is nucleation rate (nuclei/m^3/s), K is the reaction kinetic factor, k is Boltzmann constant, T_K is absolute temperature in ^0K

CNT describes two processes occurring during the formation of small nuclei of precipitation in the large volume of supersaturated solution: 1) a change in free energy at the surface of the precipitating nucleus (interfacial free energy, ΔG_s), and 2) the change in the free energy of the bulk of solution occurring during phase transition (ΔG_v), represented as function of supersaturation (S) and volume of molecular unit (v) $\frac{kTlnS}{v}$ (Nielsen, 1984):

$$\Delta G = \Delta G_s + \Delta G_v \quad (2)$$

The first term is always positive and describes the barrier to nucleation, and the second term is negative for supersaturated solution representing the driver of nucleation. There are 3 specific cases of nucleation: primary homogeneous, where the initial nucleus is considered to be a small particle of spherical shape; primary heterogeneous, where the nucleus is assumed to be hemispherical on a surface of a larger particle; and secondary, when the nucleus is formed on a plane surface of the pre-existing crystal (Karthika et al., 2016). These geometrical considerations could be taken into account to derive the exact description of ΔG (***Table 2***).

Table 2: Description of the physicochemical processes involved in free energy change for the three specific cases of nucleation

	Primary Homogenous	Primary Heterogeneous	Secondary
Assumed geometry of the system	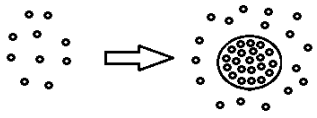	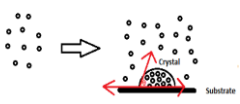	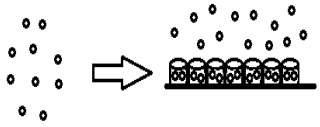
Overall ΔG	$4\pi r^2\lambda + \frac{4}{3}\pi r^3\Delta G_v$	$2\pi r^2\lambda + \frac{2}{3}\pi r^3\Delta G_v$	$2\pi rh\lambda + \pi r^2 h\Delta G_v$

Critical particle radius[3] (r_c)	$\frac{2\lambda v}{kTlnS}$	$\frac{\lambda v}{kTlnS}$	$\frac{-\lambda v}{kTlnS}$
Critical energy threshold [4] (ΔG_{crit})	$\frac{16\pi\lambda^3 v^2}{3(kTlnS)^2}$	$\frac{8\pi\lambda^3 v^2}{3(kTlnS)^2}$	$\frac{\pi h\lambda^2 v}{kTlnS}$
Interfacial free energy (λ)	1	$(\lambda_{sl} - \lambda_{sc})/\lambda_{cl}$	1
References	(De Yoreo, 2003)	(Y. Liu, Wu, Sethuraman, & Nancollas, 1997)	(Mullin, 2014)

When considering thermodynamic free energy requirements for a system with primary heterogeneous or secondary nucleation, the geometric constrains can be supplemented with additional pre- and post-exponential factors modifying the rate of nucleation equation (1) to account for the foreign particle properties and the interaction dynamics of the nucleating particle with the foreign particle or pre-existing crystal. In such cases, the theoretical primary homogeneous nucleation ΔG_{Homo} was often estimated first, and then the modifier was introduced to account for lowering the free energy value to represent heterogeneous nucleation. Such modifiers can be a constant, which proportionally lower the energy barrier (Olson, Chung-Shuan Inst. of, & Tech, 2000; Poduri & Chen, 1996), or a function *f(m,x)* that depends on the interaction and structural match between the crystal and foreign particle *m*, and the relative radius of the foreign particle *x* (Brar, France, & Smirniotis, 2001; Liu, 1999). The new energy barrier can be estimated as $\Delta G_{Hetero} = \Delta G_{Homo} \cdot (f(m,x))$, after which the contribution of *f(m,x)* can be accounted for in calculating the rate of nucleation (Liu, 2001; Liu, 2001).

The pre-exponential factor can also be modified through factors proportional to number and properties of foreign particles (Söhnel & Mullin, 1988) or by including the precipitate stoichiometry based probability constant (*F*), developed by Boistelle and Lopez-Valero (Boistelle & Lopez-Valero, 1990):

[3] Critical particle radius is achieved by setting the overall excess free energy of nucleation equation derivative to zero

[4] Critical nucleation energy threshold is achieved by substituting critical particle radius into the overall excess free energy of nucleation equation and solving for ΔG

$$F = \frac{(\beta_1+\beta_2+\beta_3\ldots\beta_n)![C_1]^{\beta_1}[C_2]^{\beta_2}[C_3]^{\beta_3}\ldots[C_n]^{\beta n}}{\beta_1!\beta_2!\beta_3!\ldots\beta_n!([C_1]+[C_2]+[C_3]\ldots+[C_n])^{\beta_1+\beta_2+\beta_3\ldots+n}} \quad (3)$$

where β_n is the balanced equation value for 'n' ion, and $[C_n]$ is concentration of 'n' ion [M]

Thermodynamic models, with the CNT framework, were widely used to describe crystallization in various biological systems such as in bone tissue engineered implants (Abdelkebir et al., 2012), additives in alkaline soil (Wang, Ruiz-Agudo, Putnis, Menneken, & Putnis, 2012), and wastewater treatment (Isopescu, Mateescu, Mihai, & Dabija, 2010), where the experimental data were shown to be in good agreement with theoretical data of calcium carbonate precipitation (Xiang Yang Liu, 2001; X. Y. Liu, 2001).

2.4.2 Kinetic theory - diffusion-reaction approach

When crystal growth rather than initial crystallization steps was of main interest, the deposition of precipitate was considered as a diffusion process from the bulk of the solution (Noyes & Whitney, 1897). Crystal growth (Ψ) can be expressed by concentration differences between the interface surface and the bulk solution as:

$$\Psi = k_m L_{SA}(c_o - c^*) \quad (4)$$

where Ψ is crystal growth rate ($mol/m^3/s$), k_m is the coefficient for mass transfer, L_{SA} is the surface area of the crystal, c_o is the solute concentration in solution, and c^* is the equilibrium concentration

The diffusion theory of crystal growth was further developed by including a reaction step of arranging the molecules into crystal lattices that follows the diffusion step of transporting solute from the fluid to the surface (Berthoud, 1912). Each of the two steps is described by equation (5), where k_m was modified to k_d for the mass transfer by diffusion or k_r for surface reaction and the driving force $(c_o - c^*)$ was divided into $(c - c_o)$ for the concentration difference between the solution and crystal-solution interface and $(c^* - c)$ for the concentration difference between the crystal-solution interface and equilibrium (saturation). The overall crystal growth formula can be derived from these equations in the form:

$$\Psi = K_G L_{SA}(c_o - c^*)^g \quad (5)$$

where K_G takes into consideration k_d and k_r, L_{SA} is the surface area of the crystal, c_o is the solute concentration in solution, c^* is the equilibrium concentration, and g is the order of

overall crystal growth processes which reflects the contribution of reaction process to the diffusion process

Originally, diffusion reaction theory assumed that the components of the precipitate are present in the solution in proportional amounts. However, this was commonly not the case, and actual aqueous concentrations of the ionic components of the potential precipitate needed to be accounted for. This is specifically relevant to precipitation of calcium phosphate as multiple potential precipitates are possible. Nancollos and Koutsoukos proposed a modification for the diffusion-reaction equation to describe the chemical reactions among precipitating ions and their relative proportions in solutions, which could be further generalized to include the effective and equilibrium concentrations of separate ion associations/dissociations (Nancollas & Koutsoukos, 1980).

$$\Psi = -K_c s \left[\left(\left[{I_{Af}}^{e+} \right]^{w+} \left[{I_{Bf}}^{e-} \right]^{w-} \right)^{\frac{1}{w}} - \left(\left[{I_{A0}}^{e+} \right]^{w+} \left[{I_{B0}}^{e-} \right]^{w-} \right)^{\frac{1}{w}} \right]^{\eta} \quad (6)$$

where Ψ is crystal growth rate ($mol/m^3/s$), K_c is the precipitation rate constant, s is the total number of nucleation sites available, $I_{(A,B)f}$ is the newly formed acidic (A) or basic (B) ion concentration, $e^{(+,-)}$ is the charge of positively or negatively charged ions, $w^{(+,-)}$ is the total number of cationic (+) or anionic (-) species, w is the sum of cationic and anionic species, $I_{(A,B)o}$ is the initial concentration of acidic (A) or basic (B) ion concentration in solution, and η is the crystallization rate modifier

2.4.2.1 Diffusion-reaction properties – Ostwald's Rule

Understanding how the biological microenvironment and time influenced the formation of different CPs is critical to predict correct precipitation dynamics. According to Ostwald's rule, the least thermodynamically stable seeded crystalline phase will always be formed prior to the next seeded crystalline phase, due to the nucleation threshold of the latter being more energetically favourable (Ostwald, 1900). Thus, Ostwald's rule assumes only the most energetically favourable crystalline phase will be formed by homogeneous nucleation, where subsequent phases of calcium precipitates will be precipitated through heterogeneous nucleation (De Yoreo, 2003). Experimental studies demonstrated the thermodynamic favourability of CPPs formation depended on pH, temperature and Ca/P ratio (Mullin, 2001). The most stable crystalline phase of CPPs, HaP, is predominately found in biology due to environmental

conditions favouring HaP precipitation. Other factors, such as protein nucleators and tissue types, can regulate the transfer of metastable CPPs, as it was shown that during blood vessel calcification, intermediate phases precede HaP formation (Murshed & McKee, 2010), while during bone mineralization, only HaP was formed (Blair et al., 2017). Therefore, when modelling biological calcium phosphate precipitation, the researchers should exercise caution and build CPP species transition based on the available experimental data.

2.4.3 Metastable-State Phase Transformation During Crystallization

Phase transformation fraction (Φ) was used to describe the transformed crystalline solid of transitioning metastable CPs (Wong & Czernuszka, 1993). The transformation of crystalline phases was classified by the nucleation of new particles that grow at a constant rate, until two nuclei impede each other after growing for a specified time. The phase transformation fraction between the final stable CP and the previous metastable CP, such as OCP crystals transitioning to HaP crystals, can be determined by considering nucleation (1) and growth (5) rates over time. These rates are modified by the transformation mechanism factor (η), which changes the rate at which the CPs nucleate and grow, depending on the availability of metastable nucleators (Christian, 1975). Once nucleators and growth of the metastable state are halted, the transformed fraction from metastable CP to stable CP can be calculated. Taken from equation's (1) and (5), nucleation (N) and growth (Ψ) were coupled as one entity (Wong & Czernuszka, 1993):

$$\Phi = 1 - \exp\left[-(\pi/3)N^{\frac{\eta}{4}}\Psi^{\frac{3\eta}{4}}t^{\eta}\right] \cdot 100 \quad (7)$$

where Φ is phase transformation fraction (Percent), N is nucleation rate ($nuclei/m^3/s$), Ψ is growth rate ($mol/m^3/s$), t is time (s), η is the crystallization rate modifier [4 = increasing or constant; 3-4 = decreasing or no presence of nucleation]

Phase transformation fraction can be used when determining the various CP states involved in the precipitation process, as well as their respective masses. This can be critical in determining pathological mineralization, such as fibrous dysplasia of the jaw bone, where brushite crystals coexist with HaP crystals (Yamamoto & Sakae, 1987).

2.5 Additional Considerations: Aqueous Phase Reactions

Supersaturation of a system with regard to species comprising precipitate, such as calcium, phosphate and hydroxide, is a prerequisite for precipitation. Supersaturation describes the state of solution in which more of the solute is contained than could be dissolved in the solvent under specific temperature and pressure (Nielsen, 1984). The supersaturated state can be achieved by increasing solute concentrations, changing temperature or pressure, all of which can be altered in the biological microenvironment in the form of changes in ion concentration, pH, temperature, or exposure to high altitude. I assessed papers for supersaturation and found that the majority of papers calculated supersaturation (92/114), with 22 of the 114 assuming supersaturation was achieved. I found that only 33 of the 114 studies explicitly modeled aqueous phase reactions.

2.5.1 Aqueous Phase Reactions

To characterize supersaturation, the events occurring in the aqueous phase need to be specified and considered, such as reactions among aqueous phase species relevant to precipitate formation (***Table 3***).

Table 3: Relevant aqueous species found in biologically relevant solutions

Aqueous Species		
Calcium	Phosphate	Hydrogen
Ca^{2+}	${PO_4}^{3-}$	H_2O
$CaOH^+$	${HPO_4}^{2-}$	H^+
${CaPO_4}^-$	${H_2PO_4}^-$	OH^-
$CaHPO_4$	H_3PO_4	
${CaH_2PO_4}^+$		

In the aqueous environment, chemical species are formed in acid-base and ion pairing reactions of the components (Oliveira et al., 2007; Szilágyi, Muntean, Barabás, Ponta, & Lakatos, 2015). The reactions among calcium and other constituents immediately relevant to the formation of CPs, such as phosphate or carbonate, need to be taken into account. Some aqueous phase chemical reactions relevant to physiological body fluid are given in (***Table 4***).

Table 4: Examples of chemical reactions relevant to the environment of physiological body fluid

Chemical Reaction	Component	Component	Species
$H^+ + OH^- \leftrightarrow H_2O$	H^+	OH^-	H_2O
$Ca^{2+} + OH^- \leftrightarrow CaOH^+$	Ca^{2+}	OH^-	$CaOH^+$
$Ca^{2+} + {PO_4}^{3-} \leftrightarrow {CaPO_4}^-$	Ca^{2+}	${PO_4}^{3-}$	${CaPO_4}^-$
$H^+ + {PO_4}^{3-} \leftrightarrow {HPO_4}^{2-}$	H^+	${PO_4}^{3-}$	${HPO_4}^{2-}$
$H^+ + {HPO_4}^{2-} \leftrightarrow {H_2PO_4}^-$	H^+	${HPO_4}^{3-}$	${H_2PO_4}^-$
$Ca^{2+} + {CO_3}^{2-} \leftrightarrow CaCO_3$	Ca^{2+}	${CO_3}^{2-}$	$CaCO_3$
${HCO_3}^- \leftrightarrow H^+ + {CO_3}^{2-}$	H^+	${CO_3}^{2-}$	${HCO_3}^-$

To account for the changes in chemical concentrations in aqueous phase, different approaches can be taken (Barat et al., 2011; Hanrahan, 2010; Musvoto, Wentzel, Loewenthal, & Ekama, 2000; Loewenthal, 1989). Nevertheless, all the approaches follow several common principles, which include the assumption that aqueous phase reactions occur much faster than precipitation, allowing chemical equilibrium to be reached in the solution; the law of mass conservation for each species and law of net charge neutrality for each aqueous phase reaction has to be maintained. Two practical approaches include the equilibrium-based (Barat et al., 2011; Loewenthal, 1989) and kinetic based modelling (Musvoto et al., 2000).

The equilibrium-based model assumes that the ion pairing transpires instantaneously, effectively removing any reaction kinetics and simplifying mathematical calculations. In contrast, the kinetic-based modelling approach provides chemical dissociation equations for the forward and reverse reaction of each weak acid/base component. For example, the transformation in the reaction between hydrogen, hydrogen phosphate and dihydrogen phosphate $H^+ + {HPO_4}^{2-} \leftrightarrow {H_2PO_4}^-$ will be written in the form for equilibrium approach $K_p = \frac{[{PO_4}^{3-}][H^+]^2}{[{H_2PO_4}^-]}$, where K_p is an apparent equilibrium constant, and for kinetic approach as $K_p' = \frac{[{HPO_4}^{2-}][H^+]}{[{H_2PO_4}^-]}$, where $K_p{}'$ is the ratio of reverse and forward reactions. Then, for equilibrium approach one needs to account for all species and components in the system and develop a set of similar equations following the general form of

$$Q_i = K_i \prod_{i=1}^{N_c} {x_j}^{a_{ij}} \quad (8)$$

where Q_i is the effective concentration of the species, K_i is an apparent equilibrium constant (also called stability constant), a_{ij} is the stoichiometric coefficient of the j^{th} component of the i^{th} species and N_c is the number of components considered

For kinetic approach the reactions considered need to be specified, and the equilibrium approximation for each reaction is written. The equilibrium approach is slightly computationally faster when large number of reactions is considered, while the kinetic based approach is more intuitive and naturally combines with the description of biological and physical processed. Nevertheless, these approaches are quite similar, and in the ranges of physiologically relevant chemical concentrations produce near identical results.

Activity coefficients are used in thermodynamics to calculate effective concentrations of each species in a complex mixture (Debye & Hückel, 1923). The activity coefficient is required to describe the relationship between the effective concentration and the molar concentration of the species, which acts as a modifying factor that depends on the environmental conditions.

$$Q_\theta = \gamma_\theta \cdot C_\theta \tag{9}$$

where C is the molar concentration, Q is the effective concentration, γ is the activity coefficient, and θ represents species (i) or component (j)

The activity coefficient depends on the solution ionic strength (I), which in turn takes into account the concentration and charge of ions present within the solution (Debye & Hückel, 1923).

$$I = \frac{1}{2}\sum_{i=1}^{n} C_i {z_i}^2 \tag{10}$$

where c_i is molar concentration and z_i is charge of each ion unit, n is the number of ion units in solution

For ionic strength, both molarity (M, mol/L, moles of solute per volume of solution) and molality (m, mol/kg, mols of solute per mass of solvent) can be used to describe ionic strength. Molarity is used when the temperature of the solution does not change. However since temperature affects the solution volume, molality rather than molarity should be used when temperature needs to be taken into account (Solomon, 2001).

The activity coefficient theoretical description was first developed in the Debye-Huckel theory (Debye & Hückel, 1923) for low ionic strength solutions, and later modified by Davies (Davies,

1962) to account for more concentrated solutions. Debye-Huckel and Davies equations formed the basis for extensions of the Debye-Huckel theory (Debye & Hückel, 1923), B-dot (Helgeson, 1969), and Pitzer (Pitzer, 1973) equations, which can also be used to describe activity coefficients. (***Table 5***).

Table 5: Sample of equations describing activity coefficients

Debye-Huckel	$log\gamma_i = -1.824 \cdot 10^6 {z_i}^2 \left(\frac{\sqrt{I}}{(\epsilon T_K)^{3/2}}\right)$
Davies Equation	$log\gamma_i = -A{z_i}^2 \left(\frac{\sqrt{I}}{1+\sqrt{I}} - 0.3I\right)$
Extended Debye-Huckel	$log\gamma_i = -A{z_i}^2 \left(\frac{\sqrt{I}}{1+aB\sqrt{I}}\right)$
B-dot	$log\gamma_i = -A_\gamma {z_i}^2 \left(\frac{\sqrt{I}}{1+a_i B_\gamma \sqrt{I}} - \dot{B}I\right)$

where γ_i is activity coefficient of each ion, A is the temperature-dependent activity coefficient constant, z_i is charge of each ion, I is ionic strength of the solution, is the relative dielectric constant for the solution, T_K is temperature of the electrolyte solution, a is the diameter of the species, B is the Debye-Huckel parameter, and $\dot{B}$ is the B-dot parameter

The effect of temperature on the activity coefficient constant A for water as a given solvent was formulated by Debye-Huckel (Debye & Hückel, 1923) as $A = \frac{1.82455 \cdot 10^6}{(DT_c)^{3/2}}$, where D is the value of the dielectric constant of water and T_c is temperature. By averaging experimentally measured dielectric constant of water, the dependence of A on temperature can be represented as: $A = 0.486 + 6.07 \cdot 10^{-4} T_c + 6.43 \cdot 10^{-6} {T_c}^2$ (H. Drake, W. Pierce, & T. Dow, 1930; Wyman, 1930).

The mass balance conservation is essential in maintaining the balance of materials that flow in and out of the physical system, so that the total input mass is equivalent to the total output mass. The equation for mass balance conservation is given in equation (11).

$$M_T = \sum_{i=1}^{N_{sp}} a_{ij} C_i \tag{11}$$

where M_T is the total mass of j^{th} component, N_{sp} is the number of species considered, a_{ij} is the stoichiometric coefficient of the j^{th} component in the i^{th} specie, and C_i is the concentration of i^{th} specie

The output generated from the mass balance equilibrium must also adhere to net electro-neutrality requirements, such that the net charge results in a neutral balance (zero). An example below using the hydrogen/phosphate system demonstrates the balance with a net charge of zero between cations and anions.

$$[H^+] = [PO_4{}^{3-}] + [HPO_4{}^{2-}] + [OH^-] + [H_2PO_4{}^-] \quad (12)$$

2.5.2 Supersaturation

Supersaturation for CPs considers the ratio between aqueous phase ion product for CP components and its solubility product (Boistelle & Lopez-Valero, 1990; Helt, 1976). The ion product of effective aqueous phase concentrations of precipitating ions is calculated as $Q_T = K_i \prod_{i=1}^{N_c} x_j{}^{\beta j}$, where x_j are components of the CP and β_j is the balancing equation value for each x_j. When the CPP is present as a solid phase in the aqueous solution, with time the equilibrium between solid and aqueous phase will be established. The solubility product (K_{sp}) is the product of such equilibrium aqueous phase ion concentrations (C_j) raised to the power of balancing coefficients $K_{sp} = K_i \prod_{i=1}^{N_c} C_j{}^{\beta_j}$. Then the supersaturation (S) can be calculated as follows:

$$S = \frac{([C_1]\gamma_1)^{\beta_1}([C_2]\gamma_2)^{\beta_2}([C_3]\gamma_3)^{\beta_3}\ldots([C_n]\gamma_n)^{\beta_n}}{K_{sp}} \quad (13)$$

where β is the balanced equation value for 'n' ion, $[C_n]$ is concentration of 'n' ion [M], γ_n is the activity coefficient of each ion, K_{sp} is Solubility constant $[mol/dm^3]$ *, and S is Supersaturation* $[mol/dm^3]$

The ratio of the effective concentration (Q_T) over the solubility product defines the critical threshold for inducing the supersaturated state in a solution. The solution is undersaturated when Q_T is less than K_{sp} (S < 1) and no precipitation should occur. The solution is supersaturated when Q_T is higher than K_{sp} (S > 1), theoretically allowing the formation of calcium phosphate precipitation.

2.6 Conclusion

This scoping review provided a general outlook on the existing literature of modelling calcium precipitation in biologically relevant systems. The three major biological systems that studied calcium precipitation were water research, agricultural sciences, and human biology. The majority of CPs studied were classified as CPPs; however, only half of the studies modelling CPP precipitation accounted for the existence of multiple related precipitates. The most predominant level of modelling within the biological systems was bioprocess models; however, general and tailored models were also significantly represented. While many earlier studies focused on nucleation or growth of CPs, more recent studies aimed to take both aspects into account, using the combination of CNT and kinetic theories. Lastly, since calcium precipitation requires the presence of a supersaturated state, most studies calculated supersaturation; however, aqueous phase reactions were not modeled in the majority of studies. Finally, the attempts to theoretically describe both biological and physicochemical aspects of the process were rare. I conclude that mathematical models that describe chemical reactions in the aqueous phase, physicochemical process of CP precipitation, as well as biological transformations, are required.

Chapter 3: Mathematical Modelling of Physicochemical Aspects of Hydroxyapatite Precipitation during Bone Mineralization

3.1 Background

Precipitation of calcium phosphate is critical for forming the inorganic matrix during bone mineralization. Together with other ionic minerals, such as hydroxide and carbonate, and biological regulators, such as vitamin D and parathyroid hormone, bone formation results in successful mineralization with hydroxyapatite (HaP) being precipitated (Siddiqui & Partridge, 2016). Changes in these ionic minerals and concentrations lead to defective mineralization states, characterized as hypo- or hyper-mineralization of bone.

Rickets and osteomalacia are defective mineralized states, which are measured by weak or softening of the bones because of significantly decreased levels of vitamin D (Reuss-Borst, 2014). As vitamin D is an important hormone that regulates the adsorption of calcium and phosphate, decreased levels lead to low levels of calcium and phosphate – critical minerals for the formation of HaP (Islam et al., 2008). The change in these ionic minerals leads to hypo-mineralization of bone. There are cases where pathological bone mineralization is regulated by underlying protein interactions, as seen in osteogenesis imperfecta, where the mechanisms are yet to be determined.

To better understand the tightly regulated and nonlinear process of mineralization from the physicochemical perspective, the model developed in this study is an extension of the previously published mathematical model that described the changes in five key components of the mineralization process: the collagen matrix divided into naïve and mature matrix, inhibitors of mineralization, nucleating centers permitting initiation of the mineralization process, and the simplified mineral formation (Komarova et al., 2015). While the model simulated many aspects of the mineralization process, it lacked a realistic description of physicochemical processes of mineral precipitation. The description of key chemical reactions involved in HaP formation from calcium (Ca^{2+}), phosphate (PO_4^{3-}), and hydroxide (OH^-) were introduced to accurately model the physicochemical process of mineral formation.

3.2 Methods

3.2.1 Modelling Biology of Bone Mineralization

The following biological components of mineralization process were included in the model:

1. Osteoblasts were assumed to form the naïve collagen matrix (x_1) that matured in the extracellular space into mature collagen matrix (x_2) through a number of processes, such as post-translational modifications and cross-linking of collagen and noncollagenous matrix proteins (Christiansen, Huang, & Silver, 2000; Kaartinen, El-Maadawy, Rasanen, & McKee, 2002; Knott & Bailey, 1998), all grouped together to occur with a characteristic rate constant of k_1 as described by equations (1a) and (1b).

$$\frac{dx_1}{dt} = -k_1 x_1 \qquad (1a)$$

$$\frac{dx_2}{dt} = k_1 x_1 \qquad (1b)$$

2. I assumed that inhibitors of mineralization (I_x), which came from circulation or were produced by osteoblasts, were delivered through naïve collagen with the characteristic rate constant of v_1, and removed proportionally to the amount of mature collagen x_2 (accounting for inhibitors binding, masking, degradation or trapping) (Christiansen et al., 2000; Kaartinen et al., 2002; Knott & Bailey, 1998) with the rate constant of r_1 as described by equations (1c).

$$\frac{dI}{dt} = v_1 x_1 - r_1 x_2 I_x \qquad (1c)$$

3. Nucleation centers (N_B) were assumed to be essential for initiation of mineral precipitation. Collagen maturation is known to give rise to intrafibrillar nucleating centers (one per collagen molecule), while interfibrillar nucleators arise on noncollagenous matrix proteins (Goldberg, Warner, Stillman, & Hunter, 1996; Hunter & Goldberg, 1993). I assumed that nucleators appear with matrix maturation, with k_2 describing the number of nucleators per mature collagen molecule as $k_2 \frac{dx_2}{dt} = k_1 k_2 x_1$. Each nucleator was assumed to initiate mineralization only once so that with time the number of nucleators decreased proportionally to the rate at which mineralized crystals (y) appear (dy/dt), as described by equation (1d).

$$\frac{dN}{dt} = k_2 \frac{dx_2}{dt} - r_2 \frac{dy}{dt} N_B \qquad (1d)$$

4. The formation of HaP (y) was assumed to be regulated by biological components of the

system so that: a) it only occurred in the presence of the nucleators N_B, in proportion to their number and b) it was impeded in the presence of inhibitors *I,* which was empirically described using the Hill type function $G_{(I)} = \frac{b}{b+I^a}$, with *a*=10 and *b*=0.001 (Komarova et al., 2015) and to depend on physicochemical state of the system resulting in the potential rate of HaP precipitation (Ψ), further described in the following sections.

$$\frac{dy}{dt} = \Psi\left(\frac{b}{b+I^a}\right)N_B \qquad (1e)$$

3.2.2 Modelling aqueous phase species

First, the chemical reactions that involve water-soluble chemical species relevant to HaP precipitation were investigated. Only chemical reactions that included the ions involved in formation of HaP crystals (Ca^{2+}, PO_4^{3-}, and OH^-) were considered and included the following species of calcium: $CaH_2PO_4^+$, $CaHPO_4$, $CaPO_4^-$, $CaOH^+$, Ca^{2+}; phosphate: H_3PO_4, $H_2PO_4^-$, HPO_4^{2-}, PO_4^{3-}; and hydroxide: H_2O, H^+ and OH^- (Montastruc et al., 2003) (***Table 6***). Any ions that may inhibit calcium phosphate precipitation, such as magnesium (Mg^+), were assumed to be constant. Chemical components were defined so that each chemical species is represented by a product of components, while no component is represented by a product of other components (Barat et al., 2011). It was assumed that chemical reactions in the aqueous phase occur much faster than the rates of biological processes and mineral formation, and chose the equilibrium approach to evaluate the changes in chemical concentrations, characterized by equilibrium constants K_i for the forward (K_{if}) and reverse (K_{ir}) reactions (Barat et al., 2011).

Table 6: The list of chemical reactions that occur in the aqueous phases and involve Ca^{2+}, OH^-, and PO_4^{3-} ions.

	H^+	Ca^{2+}	OH^-	PO_4^{3-}	HPO_4^{2-}	$H_2PO_4^-$	H_3PO_4	H_2O	$CaOH^+$	$CaPO_4^-$	$CaHPO_4$	$CaH_2PO_4^+$	
Process[5]													Rate
A. Ca^{2+}, OH^-		-1	-1						1				$K_{CaHf}[Ca^{2+}][OH^-]$
D.		1	1						-1				$K_{CaHr}[CaOH^+]$

[5] Where A is the association and D is the dissociation of a reaction

$CaOH^+$													
A. H^+, OH^-	-1		-1					1					$K_{wf}[H^+][OH^-]$
D. H_2O	1		1					-1					$K_{wr}[H_2O]$
A. $H^+, {PO_4}^{3-}$	-1			-1	1								$K_{H1f}[H^+][{PO_4}^{3-}]$
D. ${HPO_4}^{2-}$	1			1	-1								$K_{H1r}[{HPO_4}^{2-}]$
A. $H^+, {HPO_4}^{2-}$	-1				-1	1							$K_{H2f}[H^+][{HPO_4}^{3-}]$
D. ${H_2PO_4}^-$	1				1	-1							$K_{H2r}[{H_2PO_4}^-]$
A. $H^+, {H_2PO_4}^-$	-1					-1	1						$K_{H3f}[H^+][{H_2PO_4}^-]$
D. H_3PO_4	1					1	-1						$K_{H3f}[H_3PO_4]$
A. ${Ca^{2+}}, {PO_4}^{3-}$		-1		-1						1			$K_{Ca1f}[{Ca^{2+}}][{PO_4}^{3-}]$
D. ${CaPO_4}^-$		1		1						-1			$K_{Ca1r}[{CaPO_4}^-]$
A. ${Ca^{2+}}, {HPO_4}^{2-}$		-1			-1						1		$K_{Ca2f}[{Ca^{2+}}][{HPO_4}^{3-}]$
D. $CaHPO_4$		1			1						-1		$K_{Ca2r}[CaHPO_4]$
A. ${Ca^{2+}}, {H_2PO_4}^-$		-1				-1							$K_{Ca3f}[{Ca^{2+}}][{H_2PO_4}^-]$
D. ${CaH_2PO_4}^+$		1				1						-1	$K_{Ca3r}[{CaH_2PO_4}^+]$

To calculate the equilibrium concentrations, the set of mass action equations, derived from forward and reverse reaction rates, describing the changes in activities of the species (X_i), were defined as the product of the activity coefficient and the concentration of the species, considered as:

$$\frac{X_{OH^-}}{X_{H^+}^{-1}} = K_{OH^-} \quad (2a)$$

$$\frac{X_{CaOH^+}}{X_{Ca^{2+}} \cdot X_{H^+}^{-1}} = K_{CaOH^+} \quad (2b)$$

$$\frac{X_{HPO_4{}^{2-}}}{X_{PO_4{}^{3-}} \cdot X_{H^+}^{1}} = K_{HPO_4{}^{2-}} \quad (2c)$$

$$\frac{X_{H_2PO_4{}^-}}{X_{PO_4{}^{3-}} \cdot X_{H^+}^{2}} = K_{H_2PO_4{}^-} \quad (2d)$$

$$\frac{X_{H_3PO_4}}{X_{PO_4{}^{3-}} \cdot X_{H^+}^{3}} = K_{H_3PO_4} \quad (2e)$$

$$\frac{X_{CaPO_4{}^-}}{X_{PO_4{}^{3-}} \cdot X_{Ca^{2+}}} = K_{CaPO_4{}^-} \quad (2f)$$

$$\frac{X_{CaHPO_4}}{X_{PO_4{}^{3-}} \cdot X_{Ca^{2+}} \cdot X_{H^+}^{1}} = K_{CaHPO_4} \quad (2g)$$

$$\frac{X_{CaH_2PO_4{}^+}}{X_{PO_4{}^{3-}} \cdot X_{Ca^{2+}} \cdot X_{H^+}^{2}} = K_{CaH_2PO_4{}^+} \quad (2h)$$

3.2.2.1 Activity Coefficient

To determine how active each individual ion is in a mixture of chemical substances, the activity coefficient of each individual ion is calculated (Debye & Hückel, 1923). The coefficient modifies concentration of each species depending on its valence electrons (Szilágyi et al., 2015) and the ionic strength of the solution. The ionic strength (*I*, *mol/kg*) describes the combined measure of ion concentration in the solution based on their individual concentrations (c_i, *M*) and charge (z_i) (Lu & Leng, 2005; Wang et al., 2012; Xie et al., 2006).

$$I = \frac{1}{2}\sum_i c_i {z_i}^2 \quad (2i)$$

The activity coefficient equation changes the individual ion activity from the standardized chemical equilibrium reaction state (at 25^0C) to the appropriate physiological reaction state of 37^0C, and relates ion involvement to the ionic strength of the solution. The activity coefficient of each ion (γ_n) is calculated vanes on the activity coefficient constant (*A*) and the ionic strength (*I*), using the modified Debye-Huckel equation (Davies, 1962), which assumes that ions are spherical, that complete dissociation of ions and no partial associations between ions is present within the system. This activity coefficient equation is valid till ionic strengths of 0.5M, and can be used to

accurately describes the activity of ions in physiological solution, since physiological ionic strength rarely surpasses 100 mM (Davies, 1962; Helt, 1976).

$$\log \gamma_i = -Az_i^2 \left[\frac{I^{0.5}}{1 + I^{0.5}} - 0.3I \right] \qquad (2j)$$

The activity coefficient (A) in equation (2j) is the factor describing the effect of temperature on ionic activity. The empirical relationship between the activity coefficient and the temperature (T_C, ^oC) has been established (Manov, Bates, Hamer, & Acree, 1943; Rice et al., 2010):

$$A = 0.486 + 6.07 \cdot 10^{-4} T_c + 6.43 \cdot 10^{-6} T_c^2 \qquad (2k)$$

3.2.2.2 Mass Balance Conservation

The mass balance conservation describes the flow of material within the system. I assume that within the characteristic times for aqueous phase equilibrium, the total concentrations of Ca^{2+}, PO_4^3 and OH^- (or H^+) in all related chemical species remains constant. When HaP is precipitated, I calculate the outflow of Ca^{2+}, PO_4^3 and OH^- from the system, however I assume that since HaP precipitation is much slower than ion diffusion and equilibrium, the influx of Ca^{2+}, PO_4^3 and OH^- from surrounding space replenish these ions, thus keeping their total concentrations unchanged. The mass balance in the aqueous phase is described by equations (2l-2n):

$$T_{Ca^{2+}} = [Ca^{2+}] + [CaOH^+] + [CaPO_4^-] + [CaH_2PO_4^+] + [CaHPO_4^-] \qquad (2l)$$

$$T_{PO_4^{3-}} = [PO_4^{3-}] + [CaPO_4^-] + [CaHPO_4] + [CaH_2PO_4^+] + [HPO_4^{2-}] + [H_2PO_4^-] + [H_3PO_4] \quad (2m)$$

$$T_{H^+} = [H^+] + [CaHPO_4] + [CaH_2PO_4^+] + [HPO_4^{2-}] + 2[H_2PO_4^-] + 3[H_3PO_4] - [CaOH^+] - [OH^-] \quad (2n)$$

The set of mass action equations (2a-2h) in conjunction with the mass balance equations are used for equilibria of the aqueous phase, which consist of eleven non-linear algebraic equations, where eight follow the law of mass action, respective to the number of species involved, and three adhere to the mass balance of each component.

3.2.3 Crystal Growth

HaP formation from Ca^{2+}, PO_4^3 and OH^- is chemically described by equation (3a):

$$5Ca^{2+} + 3PO_4{}^{3-} + OH^- \leftrightarrow Ca_5(PO_4)_3OH \qquad (3a)$$

Other CPPs were disregarded for the purpose of forming bone HaP as these precipitates were not thermodynamically favourable to form bone (HaP), as per previous experiments conducted (Boistelle & Lopez-Valero, 1990; Martin, 1994; Wang et al., 2012). To calculate the rate of HaP precipitation, three processes need to be determined: 1) the degree of supersaturation needs to be established, 2) the rate of physicochemically driven precipitate formation is calculated, and 3) biological factors in the system are taken into account.

3.2.3.1 Supersaturation

The supersaturation (S) of the system describes the state of solution in which more of the dissolved material is contained than could be dissolved under standard chemical experimental conditions (Oliveira et al., 2007). Mineral is assumed to only precipitate when saturation value is above 1. The supersaturation equation for calculating the probability of HaP precipitation, where concentration of n ion (C_n) given in [M], the activity coefficient of each ion (γ_n), and the solubility constant (K_{sp}) given in [mol/dm^3], is described by equation (3b).

$$S(HaP) = \frac{([Ca^{2+}]\gamma_{Ca^{2+}})^5\left([PO_4{}^{3-}]\gamma_{PO_4{}^{3-}}\right)^3([OH^-]\gamma_{OH^-})^1}{K_{s,HA}} \qquad (3b)$$

3.2.3.2 Growth Formula

The growth formula used for precipitation was developed by Nancollos and Koutsoukos, who proposed a modification for the diffusion-reaction equation to describe the chemical reactions among precipitating ions and their relative proportions in solutions, which could be further generalized to include the effective and equilibrium concentrations of separate ion associations/dissociations (Nancollas & Koutsoukos, 1980). The growth (Ψ) formula given in [$mol/m^3/s$], where the precipitation rate constant (K_c), the total number of growth sites (N_B) available on the seeded material, the newly formed acidic and basic ion concentration ($[Ion]_f$), the stoichiometric coefficient of the ion (a_{ij}), the charge of positively charged ions (e^+), the total number of cationic species (w^+), the charge of negatively charged ions (e^-), the total number of anionic species (w^-), the sum of cationic and anionic species (w), the initial concentration of

acidic and basic ion concentration in solution ($[Ion]_o$), and the crystal transformation constant (η), is described by equation (3c).

$$\Psi = -K_c N_B \left[\left(\left[{Ca_f}^{2+} \right]^5 \left[{PO_4}_f^{3-} \right]^3 \left[{OH_f}^{-} \right]^1 \right)^{\frac{1}{9}} - \left(\left[{Ca_o}^{2+} \right]^5 \left[{PO_4}_o^{3-} \right]^3 \left[{OH_o}^{-} \right]^1 \right)^{\frac{1}{9}} \right]^{\eta} \quad (3c)$$

It was assumed that ions deposited on the surface and between the collagen fibers in a manner of intrafibrillar, interfibrillar, and gaps between the ends of collagen fibers, are driven mainly by diffusion and not surface energy (Olszta et al., 2007). The growth formula does not focus on surface energy or adsorption layer as a theory for nucleation and growth and assumes that diffusion is the primary driver of crystal growth. Once nucleated, the crystals grow depending on the variation in ion concentration and. The growth formula presented in equation (3c) cannot explain the layer growth or the removal of parts of the crystal (faceting) of crystals.

3.2.4 Mineral Formation

The formation of mineral HaP was modified from the original mathematical model of Komarova *et al.* to include physicochemical kinetics in forming HaP mineral (Komarova et al., 2015). The characteristic rate (k_3) constant was modified to the currently proposed growth (Ψ) formula that accounts for concentration of ions and temperature in the calculations from equations (1-3), where $(\frac{b}{b+I^a})$ is a Hill-type function that fits the biological system being modelled, as described by equation (4a).

$$\frac{dy}{dt} = \Psi(\frac{b}{b + I^a}) \quad (4a)$$

It was assumed that the HaP mineral formed is the only calcium phosphate phase precipitated. The calcium phosphate mineral total is the total mineral content of distinct calcium phosphate precipitate in the form of HaP.

3.2.5 Characterization and Estimation of Parameters and Variables

To correctly model the aqueous phase reactions and mineral formation, uncertainty was addressed and divided into three categories: model uncertainty, parameter uncertainty, and parameter variability (Finkel, 1990). The criteria for model uncertainty included which species should be considered and what processes control the reaction. Parameter uncertainty includes the models used to adjust the thermodynamic properties involved in aqueous phase reactions, such as ionic strength, activity, and temperature. Lastly, parameter variability is the difference in experimental data and their related equilibrium constants, forward/reverse reaction constants, and solubility products.

3.2.5.1 Aqueous Phase Parameter Estimation

To estimate the correct number of aqueous phase reactions present during bone mineralization, the studies found in chapter 2 were sampled for biologically relevant systems that modeled aqueous phase reactions of calcium precipitation. From 33 studies that modeled such reactions, I identified 19 studies that were consistent with the eight reactions listed in **Table 7**. The other 14 studies modeled calcium precipitation that was not CP specific, such as calcium carbonate, which were confidently disregarded as they do not represent HaP precipitation relevant to bone mineralization. The driving forces were assumed to be driven by equilibrium rather than kinetic processes, due to the local equilibrium assumption that can be applied to the equilibrium occurring between extracellular and local environments of bone mineralization (Hanrahan, 2010). As the aqueous phase reactions are reversible and have near instant ion-pair exchanges, the equilibrium assumption falls within a 2% error of the kinetic model, with an extensive reduction in computation time and power (Ludovic Montastruc, Azzaro-Pantel, Cabassud, & Biscans, 2002). The three mass balance equations, consisting of Ca^{2+}, PO_4^{3-}, and H^+, were assumed to start with total concentrations equal to $1.21 \cdot 10^{-3}$M, $1.28 \cdot 10^{-3}$M, and $41 \cdot 10^{-9}$M, respectively, representing the average value of the physiological range determined experimentally in blood serum concentrations and interstitial fluid (Arnett, 2008; Moe, 2008).

To account for the correct number of parameters, the studies that had modeled aqueous phase reactions and thermodynamic properties were investigated. Of the 95 studies included, every study had included ionic strength, activity coefficient, and supersaturation in their models to

study calcium precipitation. Therefore, it was safe to assume that these three parameters should be included in the model. The temperature value chosen was 310 ^{0}K (37 ^{0}C), to represent the physiologically relevant temperature in the body (Obermeyer, Samra, & Mullainathan, 2017).

Parameter variability was a serious concern, especially when trying to achieve equilibrium in the aqueous phase. Equilibrium constant values of the eight aqueous phase reactions and the solubility product of HaP drastically affected the potential to equilibrate the system. As equilibrium constants are determined experimentally under different conditions, measurement error, analysis technique, and instrumentation error play a critical role in the uncertainty of the equilibrium constant values. The study that modeled the precipitation of calcium phosphate in near physiological conditions was chosen for the equilibrium constants, as it was the approximate average equilibrium constant value across the eight species and amongst the seven studies (***Table 7***).

Table 7: The list of species involved and their associated equilibrium constants

Species	Equilibrium Constant (K)
H_2O	$1.01 \cdot 10^{-14}$
$CaOH^+$	20
$CaPO_4^-$	$2.88 \cdot 10^{6}$
HPO_4^{2-}	$4.05 \cdot 10^{-13}$
$H_2PO_4^-$	$3.52 \cdot 10^{-8}$
H_3PO_4	$7.11 \cdot 10^{-3}$
$CaHPO_4$	254
$CaH_2PO_4^+$	5.1

3.2.5.2 Parameter and Variable Estimation of Biological Components

Many of the parameters and variables of the biological components originate from the previously established model (Komarova et al., 2015); thus, a brief overview of the critical components is summarized below. $9.4 \cdot 10^{5}$ molecules of collagen were calculated to fit within the matrix volume according to the diameter and length of collagen that form fibrils, as well as the respective geometry formed. The number of nucleators was assumed to be the same order as collagen

molecules (k_2) equal to 1, due to the assumption of grouped inhibition functionality and spatial limitations within the organic matrix. Rate constant values were based on the two phases of bone mineralization, where matrix maturation is longer than mineralization of the matrix. The rate of collagen assembly (k_1) was assumed to be 0.1 day^{-1}, rate of inhibitor delivery (v_1) to be 0.1 day^{-1}, rate of inhibitor degradation (r_1) to be $2 \cdot 10^7$ $day^{-1}mol^{-1}$ and the rate of nucleator use by mineralization (r_2) to be $1.5\text{-}2 \cdot 10^{-8} mol^{-1}$. The constants used in the Hill-type function strongly resembled the biological interpretation of the system and the critical inhibition value permitted in mineralization, where a = 10 and b = 0.001. All values and constants were determined experimentally by studies conducted by Boskey et al, George et al, and Murshed et al (Boskey, 1996; George & Hao, 2005; Murshed & McKee, 2010).

3.2.5.3 Mineral Formation Parameter Estimation

The growth equation was chosen due to the fact that crystal growth rather than the initial crystallization steps were the main focus of the model and subsequently better represented the biological system being modeled. Due to the fast exchange and local equilibrium assumption, I assumed that the system is saturated locally. Mineral precipitation was determined to be the difference between the ion concentrations at time (t) and the solubility product (K_{sp}) of HaP. After a similar search for the equilibrium constants, the K_{sp} was determined to be $2.5 \cdot 10^{-59}$ M^9, as this was the average of the most consistently reported values; however, it should be noted that the value of K_{sp} may range from 10^{-53} to 10^{-61} depending on the ionic strength, temperature, and Ca/P ratio of the HaP precipitated experimentally (E.C. Moreno, 1968). As resorption takes approximately 30 days and bone formation 120 days, the time chosen to simulate mineral formation was 120 days. According to Wong and Czernuszka, the nature of the growth mechanism (n) is determined by growth or interface region, where diffusion was determined to be equal to three (Wong & Czernuszka, 1993).

3.3 Results

The following displays the outcome of changing initial concentrations of calcium, phosphate, and hydrogen, and their effects on the biological and chemical processes involved in bone mineralization.

3.3.1 Aqueous Phase Concentrations at Equilibrium

The aqueous species involved in precipitating HaP were investigated at equilibrium. The chemical reactions of each species remain in an equilibrium state without HaP mineral formation due to the assumption of instantaneous ion pair reactions at the extracellular level. **Figure 6 and 7** show the concentrations of all eight aqueous phase species at equilibrium with respect to changing initial total concentrations of Ca^{2+} (1.21 mM) and PO_4^{3-} (1.28 mM), referred to as MCaT and MPO4T from now on, respectively.

Figure 6: Aqueous phase reactions at equilibrium for changing serum calcium concentration. *MatLab code for aqueous phase equilibrium was run, with MPO4T = 1.28 mM, MHT = 41nM, and MCaT starting at 0.63 mM and increasing by 0.01mM until 3.13 mM, representing the maximum pathological concentration of MCaT reported from literature. The simulation was run seven times, each with a different set of K constants retrieved from the studies listed in Appendix B. The study marked in* ***Red*** *was used in further studies calculating saturation and mineral formation.*

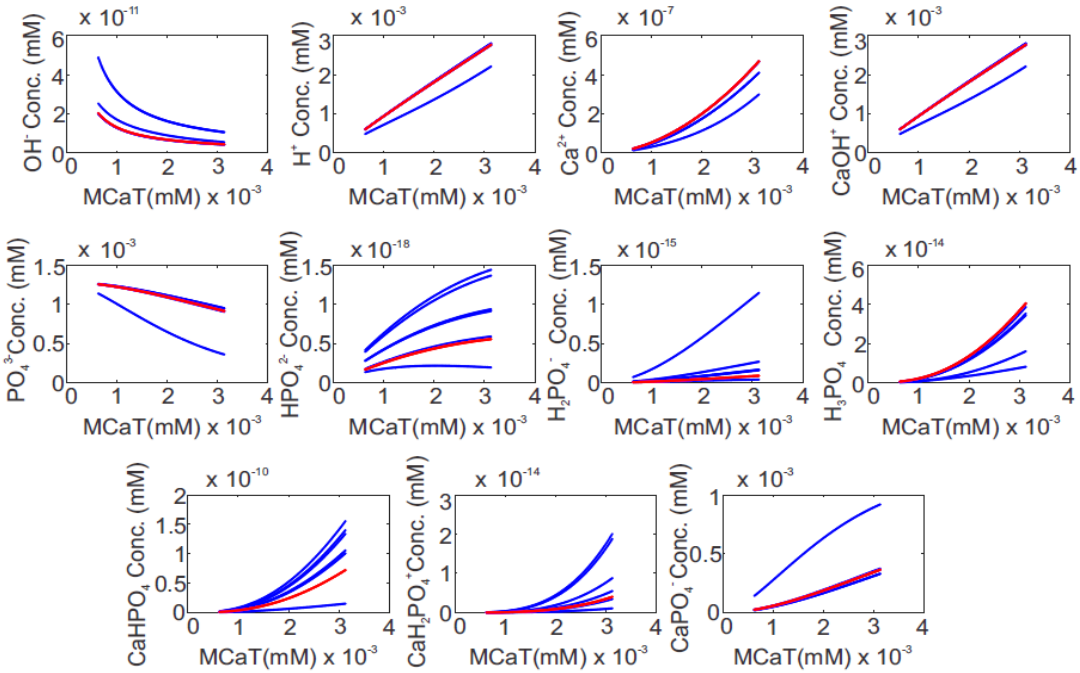

Parameter variability was investigated when attempting to achieve equilibrium in the aqueous phase. Equilibrium constant values of seven aqueous phase reactions affected the potential to equilibrate the system and the specie concentration values. As equilibrium constants are

determined experimentally under different conditions, measurement error, analysis technique, and instrumentation error play a critical role in the uncertainty of the equilibrium constant values. Of the 33 studies that included aqueous phase reactions, 20 explicitly stated their equilibrium values in either pK, (-) logK, or K format as shown in ***Table S1***. Seven out of the available 21 studies reported similar values for the included species, with another five studies reporting similar values for at least five or more of the species. There were four studies that were not consistent in equilibrium constant values. The large discrepancy is because of the reporting values during experimental procedures and carelessness in attention to detail, such as missing a negative sign or reporting logK values instead of them actually being –logK values. For example, Recillas reported similar values to the seven consistent studies; however, for their phosphate system (H_3PO_4, H_2PO^{4-}, HPO_4^{2-}), a negative sign in the 10^{th} to the power degree caused a significant change in the equilibrium constants, preventing the system from reaching equilibrium (Recillas et al., 2012). Although there was variance seen between the seven studies including the acid-base association/dissociation constant, the K value is consistent in the majority of studies (at least 5/7) for all species excluding HPO_4^{2-}, leading to the safe exclusion of outlier K values. As a result, the study that modeled the precipitation of calcium phosphate phases in near physiological conditions was chosen for the equilibrium constants, as it was the approximate average equilibrium constant value amongst the seven studies as well as closely relating to the bone mineralization environment.

The observed experimental outcome showed that increasing MCaT lead to an increase of all species with Ca^{2+} in their molecular composition. The OH^- and H^+ species concentrations followed the equilibrium of water, therefore when OH^- decreased, H^+ was increased to equilibrate at the association/dissociation constant of $1.0x10^{-14}$. Subsequently, the increase in H^+ leads to an increase in the phosphate buffering species (HPO_4^{2-}, $H_2PO_4^-$, and H_3PO_4), despite the decrease in phosphate. This is because species must adhere to le Chatelier's principle of equilibrium concentration balance and to the acid-base association/dissociation constant. PO_4^{3-} decrease during MCaT increase can be particularly explained by the species sharing Ca^{2+} and PO_4^{3-} ions, where $CaHPO_4$, CaH_2PO4^+, and $CaPO_4^-$ concentration is increased because of le Chatelier's principle and the acid-base association/dissociation constant as shown in equation (5a).

$$Ca^{2+} = \frac{CaPO_4^{-}}{PO_4^{3-}}, which\ leads\ to: Ca^{2+} \uparrow = \frac{CaPO_4^{-} \uparrow}{PO_4^{3-} \downarrow} \quad (5a)$$

It was also observed that Ca^{2+} more strongly influenced the rest of the species at equilibrium.

Figure 7: Aqueous phase reactions at equilibrium for changing serum phosphate concentration. *MatLab code for aqueous phase equilibrium was run, with MCaT = 1.21 mM, MHT = 41nM, and MPO4T starting at 0.25 mM and increasing by 0.01mM until 2.75 mM, representing the maximum pathological concentration of MPO4T reported from literature. The simulation was run seven times, each with a different set of K constants retrieved from the studies listed in Appendix B. The study marked in* ***Red*** *was used in further studies calculating saturation and mineral formation.*

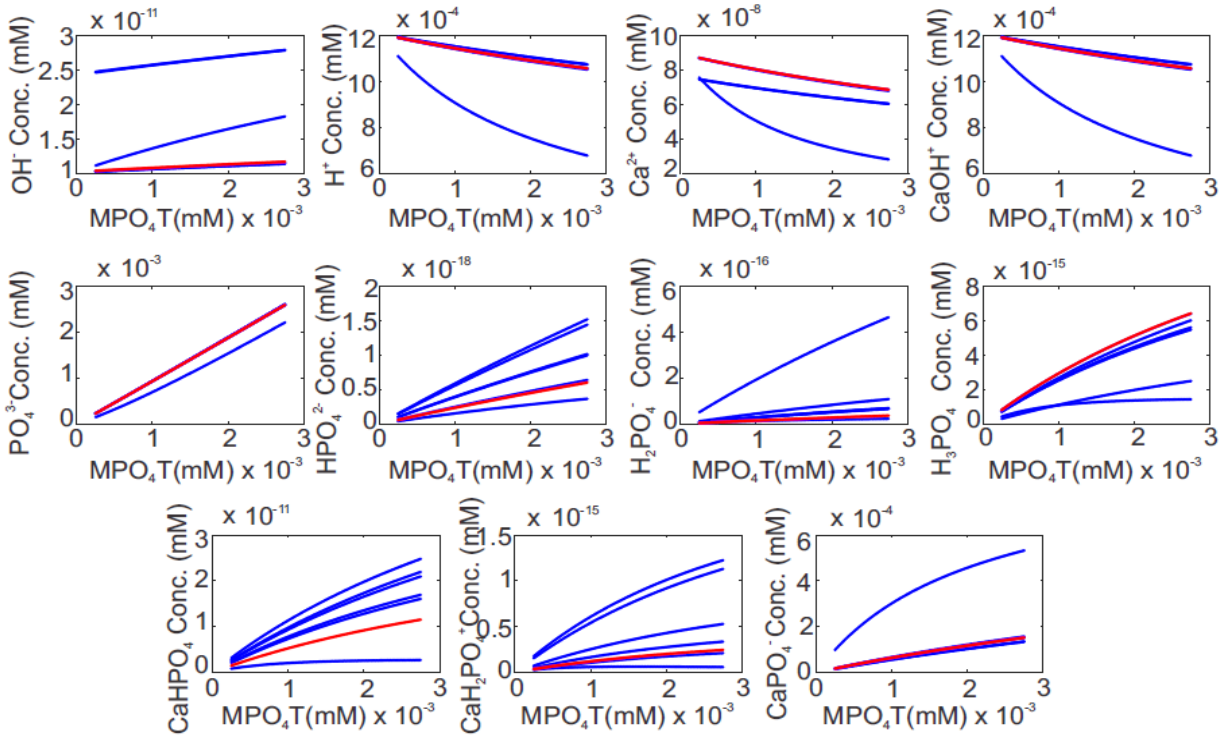

Investigating the increase in MPO4T observed in **Figure 7**, the aqueous equilibrium principles from calcium can be similarly applied. When MPO4T is increased, the phosphate species concentration is increased as well. The increase in phosphate species decreases the concentration of Ca^{2+}, following the same principles applied in **Figure 6**. Looking at the same example for

$CaPO_4^-$, Ca^{2+} must decrease in order for PO_4^{3-} to increase as per the acid-base association/dissociation constant shown in equation (5b).

$$PO_4{}^{3-} = \frac{CaPO_4{}^-}{Ca^{2+}}, which\ leads\ to: PO_4{}^{3-} \uparrow = \frac{CaPO_4{}^- \uparrow}{Ca^{2+} \downarrow} \quad (5b)$$

The increase in initial hydrogen concentration, referred to as MHT, can be explained by the same aqueous equilibrium seen in increasing MCaT. Since H^+ increases when increasing the concentration of MCaT, an increase in MHT follows the same chemical balancing principles, therefore producing an increase in H^+ and the subsequent cascading effects on the other species.

3.3.2 Supersaturation at Equilibrium

The aqueous species that react to precipitate HaP were investigated in terms of supersaturation, which is normally possible when the concentration product of ions exceeds the solubility product of the precipitate being formed. This produces the critical threshold value of 1 for supersaturation, where anything greater should lead to mineral formation and below should lead to dissolution of the mineral; however, other factors may cause mineral formation to precipitate below supersaturated levels. **Figure 8** shows the supersaturation values, with respect to the initial serum concentrations and the variation in K_{sp} for HaP values. A similar search was done for K_{sp} as it was done for the equilibrium constants and the K_{sp} was determined to be $2.35 \cdot 10^{-59}$ M^9, as this was the most consistently reported value; however, it should be noted that the value of K_{sp} may range from 10^{-53} to 10^{-61} depending on the ionic strength, temperature, and Ca/P ratio of the HaP precipitated experimentally (Moreno, 1968). In the majority of K_{sp} values, the solution was observed to be supersaturated with increasing values as initial concentrations increased; however, in one case, the solution was not supersaturated at physiologically relevant values due to the K_{sp} value ($1.69 \cdot 10^{-53}$ M^9) of HaP. This value reported by Recillas was obtained at ionic strength values far greater than what would be observed in the local bone microenvironment (0.143M compared with 0.010M) and at a temperature of 25^0C, all of which affected the ion contribution on the solution and subsequently misrepresented the K_{sp} value observed in the human body (Koutsoukos & Nancollas, 1981; Recillas et al., 2012).

Figure 8: Supersaturation values for increasing initial serum concentration values. *MatLab code for aqueous phase equilibrium was run, with baseline values of MPO4T = 1.28 mM, MHT = 41nM, and MCaT =1.21 mM. For MCaT, the value was increased by 0.01mM from 0.63mM to 3.13mM; for MPO4T, the value was increased by 0.01mM from 0.25mM to 2.75mM; for MHT, the value was increased by 0.03nM from 15.8nM to 145nM.The simulation was run five times, each with a different K_{sp} value retrieved from the studies in Appendix B. The simulation outlined in* ***Red*** *was the K_{sp} value chosen for subsequent mineral formation simulations.*

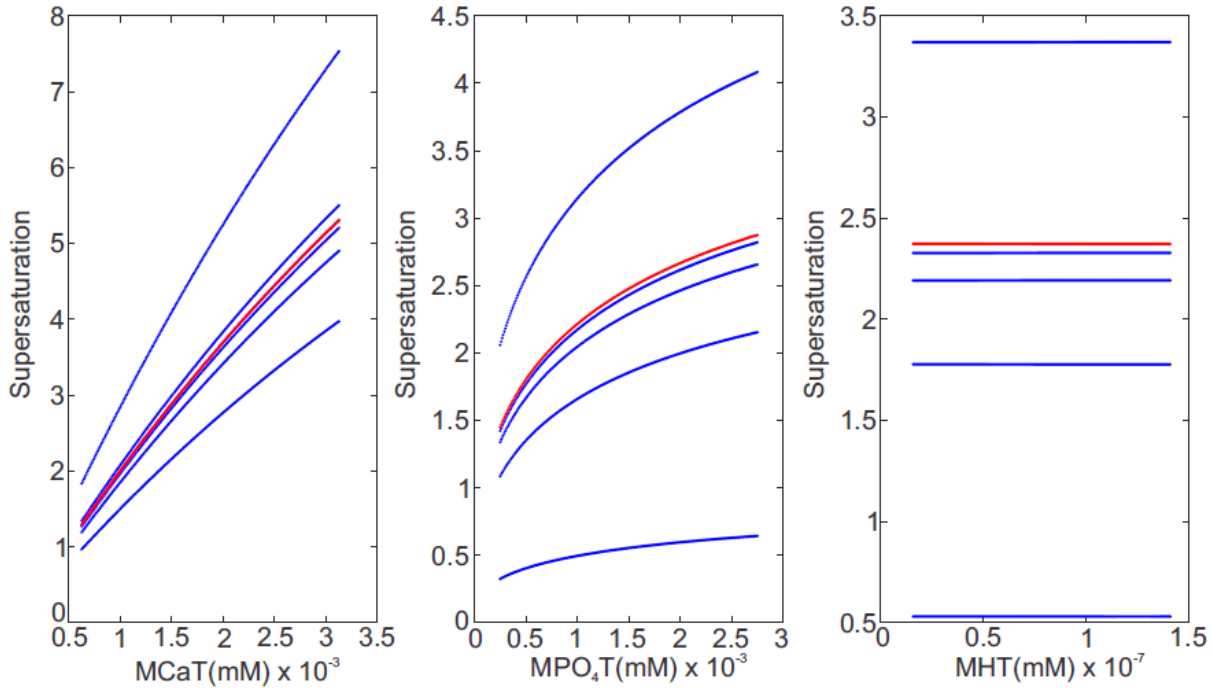

As initial concentrations were increased, the supersaturation value increased linearly for MCaT and MHT; however, the supersaturation value for MPO4T resembles the trend of a negative quadratic function. This outcome demonstrates the notable influence of Ca^{2+} on the overall system and its relationship with PO_4^{3-}. As the human body is not one solid block of mineral, this raises the question of whether the K_{sp} value of chemically precipitated HaP truly represents the HaP being formed in the body (Hassanali, Wong, Lynch, & Anderson, 2017). Further investigation into whether or not the chemical composition of HaP is the exact same mineral precipitated in the body and its relative solubility constant should be examined.

3.3.3 Chemical Mineral Formation

Once aqueous specie concentrations and supersaturation states were determined, the mineral formation of HaP could be investigated. Mineral was determined to be precipitated through the

diffusive-reactive process using Koutsokos' crystal growth equation for HaP (Nancollas & Koutsoukos, 1980). After running simulation for mineral growth, it was observed that the mineral formation over 120 days was far below the estimated density of 1200-2000 mg/cm^3 HaP in bone (Burghardt, Kazakia, Laib, & Majumdar, 2008; Sekhon, Kazakia, Burghardt, Hermannsson, & Majumdar, 2009). To investigate the amount of mineral formed and the volume HaP occupies, the precipitation constant (K_c) was changed, until a comparable amount of mineral (in grams) and volume (in m^3) to the estimated density of HaP, was observed.

Figure 9: Volume of mineral formed compared with mineral mass using the infinite supply of ions available. *MatLab code for mineral growth was run, with baseline values of MPO4T = 1.28 mM, MHT = 41nM, and MCaT =1.21 mM. The simulation was run four times, where the K value was changed until the mineral volume values were comparable to physiological ranges in human bone. The simulation outlined in* ***Red*** *was the K value chosen and was subsequently used in further studies.*

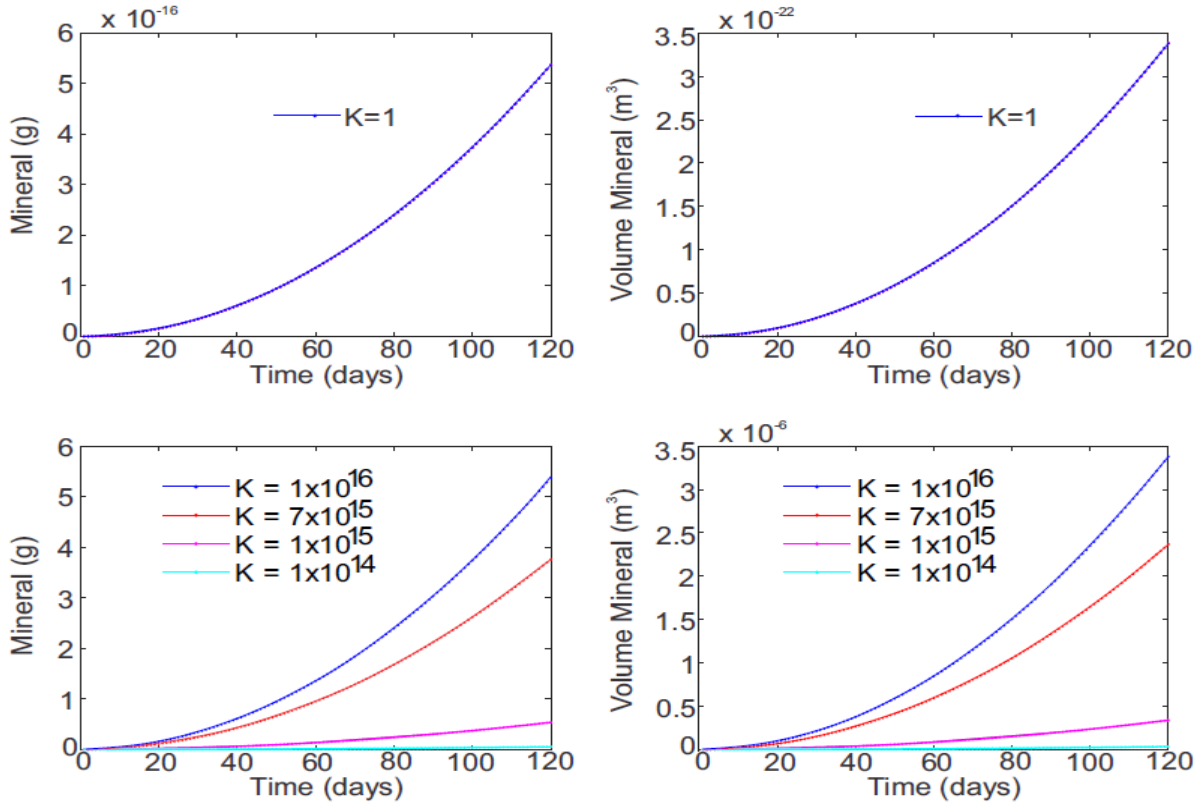

It was observed that at a precipitation constant of 7x10^{15}, the estimated density of HaP was determined to be 1.58g/cm^3 (1580mg/cm^3). The mineral and volume simultaneously increase as

the time goes on with a difference of 10^6 in mineral volume to amount of mineral formed (***Figure 9***). This is due to the decreased size of the molar mass-to-mass density ratio of HaP. The results obtained for the volume of the mineral prompted further investigation into the volume of the extracellular reservoir (where ions are stored) and whether there is an infinite supply of ions (very large volume) or whether it is limited by the availability of ions.

The amount of mineral formed with respect to changes in the extracellular volume is shown in **Figure 10**. In the presence of a very large volume ($1x10^{-9}$ m^3), comparably, the mineral amount grows indefinitely as the ions required to form HaP are saturated and the solution is constantly supersaturated. Smaller volumes were investigated at $1x10^{-12}$ m^3, $1x10^{-13}$ m^3, $1x10^{-14}$ m^3, where ion concentrations depleted faster with smaller volumes. Since the mathematical model from the previous paper determined that there is a 20-day delay before mineral formation begins to form, the volume of $1x10^{-12}$ m^3 was chosen as it was most consistent with the mineral formation dynamics previously observed. Once the precipitation constant and volume was determined, investigating the changes of MCaT and MPO4T was implemented to observe the pathological cases using only physicochemical dynamics.

Figure 10: Mineral formed compared to changes in volume. *MatLab code for mineral growth was run, with baseline values of MPO4T = 1.28 mM, MHT = 41nM, and MCaT =1.21 mM. The simulation was run four times, changing the volume for values 1000um^3, 100,000um^3, 1x10^{6}um^3, and 1x10^{9}um^3, going from lowest to largest mineral formed, respectively.*

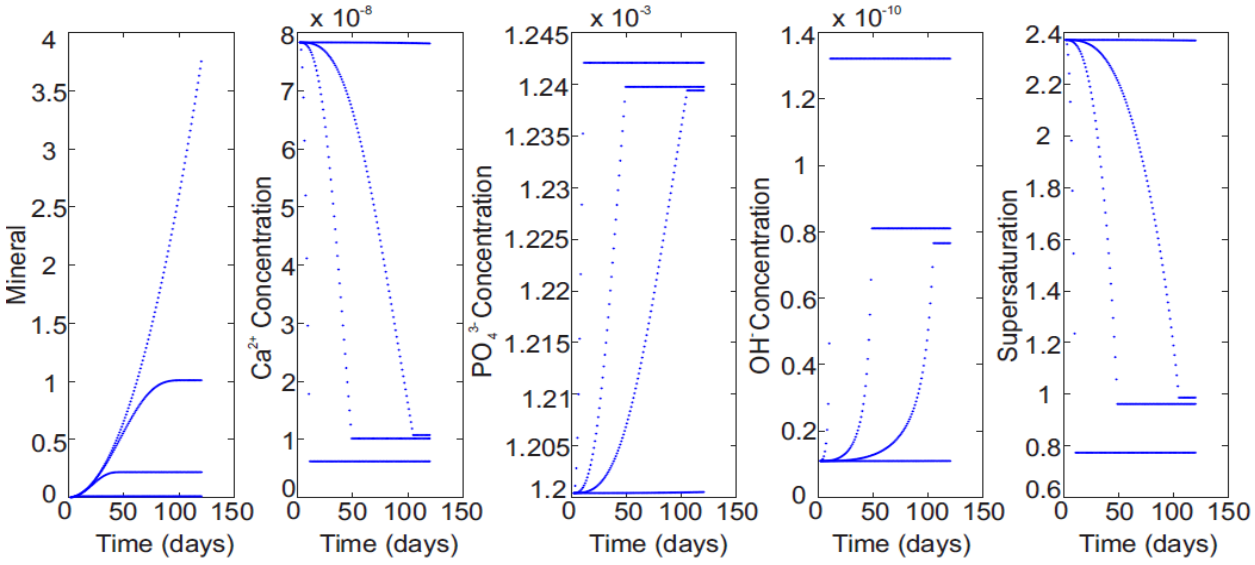

Figure 11 and 12 shows the mineral growth of HaP under baseline, minimum, and maximum ion concentrations for MCaT and MPO4T. As the solution is originally supersaturated, it was observed that mineral growth increased quicker as the concentration was increased. Baseline conditions resembled the initial slow growth of mineral production, followed by swift mineralization, and saturating around 100 days when the solution has dropped below supersaturation. When MCaT was increased to the maximum concentration seen in pathological conditions (3.1 mM), mineral growth increased quickly and saturated within 40 days at much greater amounts of mineral compared to baseline values, which is seen in hypercalcemic conditions of bone formation. Contrarily, when MCaT was decreased to the minimum concentration (0.63 mM), mineral growth slowly increased with little amount of mineral being formed over 120 days.

Figure 11: Mineral formed compared with disease states for MCaT. *MatLab code for mineral growth was run, with baseline values of MPO4T = 1.28 mM, MHT = 41nM, MCaT =1.21 mM, and V = 1x10^{6}um^3. The simulation was run three times, changing the MCaT values for the absolute minimum and maximum concentrations observed in pathology, going from lowest to largest mineral formed, respectively.*

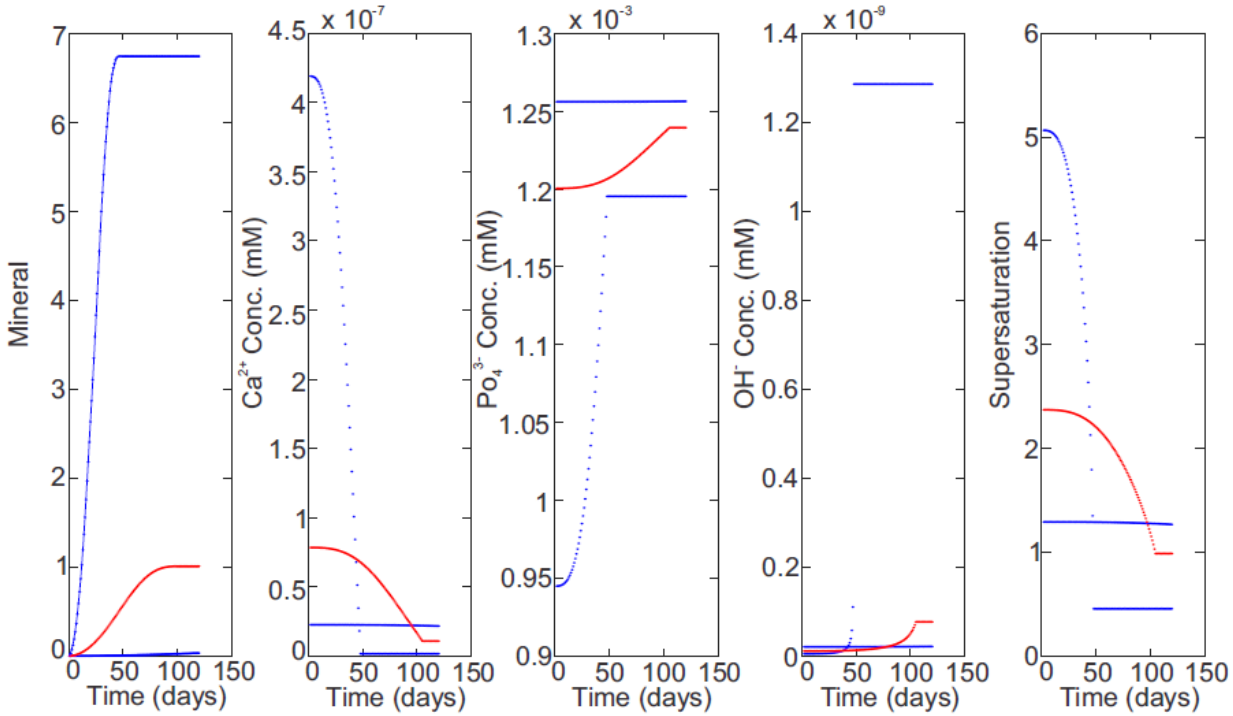

Similar dynamics were seen when MPO4T was changed to the maximum and minimum concentrations seen in pathology. The amount of mineral formed, however, was much smaller at maximum MPO4T (2.8mM) compared to maximum MCaT and slightly greater at minimum MPO4T (0.25 mM) concentrations compared to minimum MCaT, suggesting that Ca^{2+} plays a strong role in influencing the formation of HaP. This is consistent with the stoichiometric coefficients of HaP, where Ca^{2+} is the most required element in forming HaP crystals.

Figure 12: Mineral formed compared with disease states for MPO4T. *MPO4T = 1.28 mM, MHT = 41nM, MCaT =1.21 mM, and V = 1x10^{6}um^3. The simulation was run three times, changing the MPO4T values for the absolute minimum and maximum concentrations observed in pathology, going from lowest to largest mineral formed, respectively.*

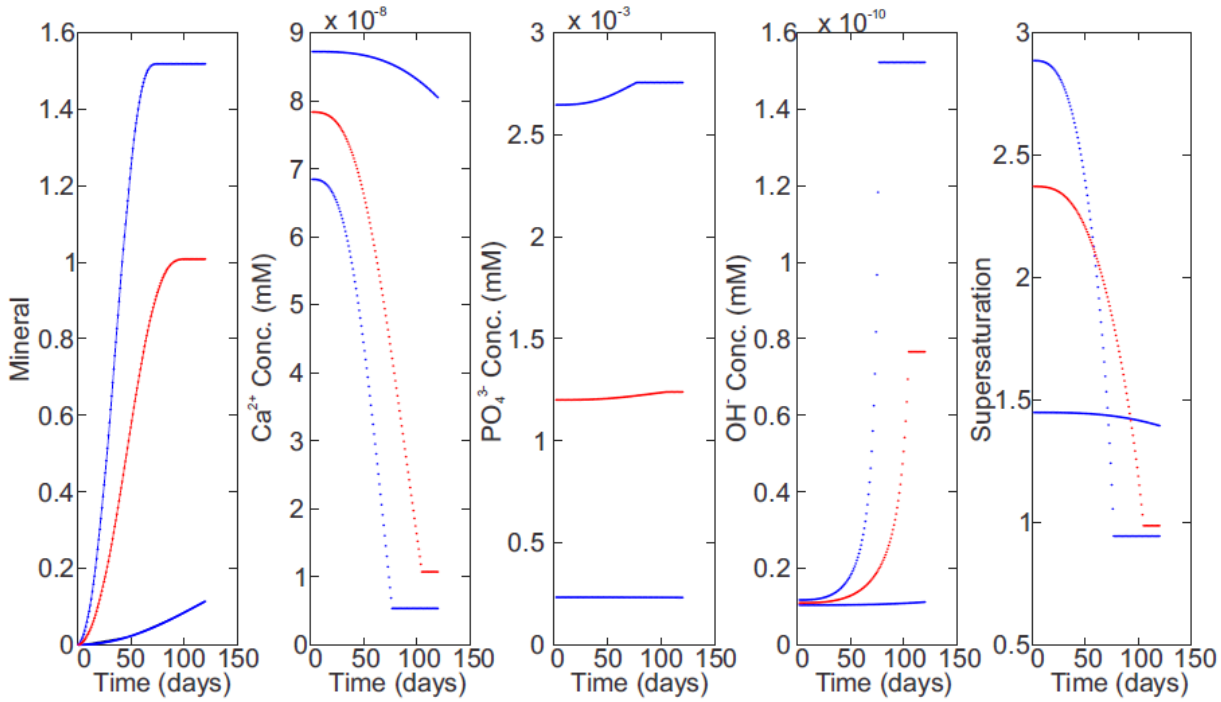

3.3.4 Physicochemical Dynamics Integrated with Biological Components of Bone Mineralization

After determining the aqueous phase dynamics in conjunction with purely chemistry-based mineral formation, the physicochemical dynamics were integrated with the biological components of bone mineralization to investigate healthy and pathological cases of bone mineralization, such as hypo- and hyper-calcemia and phosphatemia. The parameters for bone mineralization, which are naïve collagen, mature collagen, inhibitors, nucleators, and mineral,

were investigated to follow similar mineralization dynamics as presented in the previous model. Naïve collagen was converted to mature collagen (cross-linked) after 50 days with no mineral formation in the initial 10 days of collagen maturation due to the presence of inhibitors. Once sufficient mature collagen was formed, inhibitors were degraded and elevated nucleator concentration stimulated the rapid production of mineral HaP, until about 80 days, where mineral growth reached 90% of the total normalized mineralization degree and was determined to be the healthy state of mineralization. **Figure 13** shows the delayed response in mineral production, swift mineralization, and slow accumulation of mineral crystals that was preserved in the updated model with physicochemical dynamics (Roschger, Paschalis, Fratzl, & Klaushofer, 2008).

Figure 13: Physicochemical dynamics integrated with biological components for healthy bone mineralization. *Matlab code with mineral growth and biology was run simultaneously. Baseline values of MPO4T = 1.28 mM, MHT = 41nM, MCaT =1.21 mM, and V = 1x10^{6}um^3 were utilized. The simulation was run once to obtain the baseline value for healthy bone mineralization.*

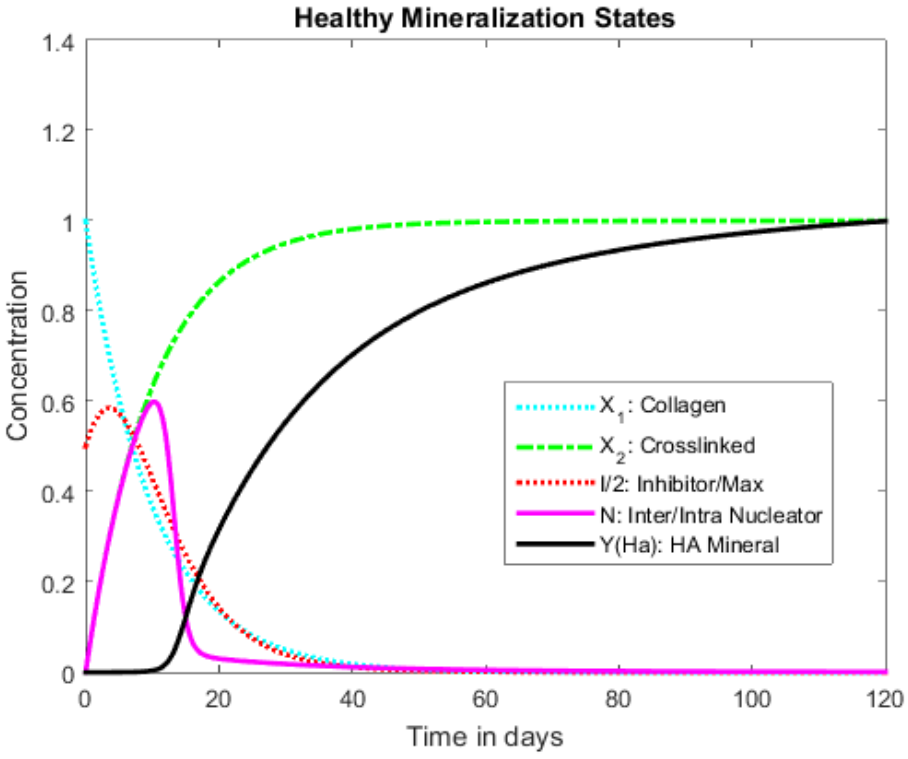

Once healthy bone mineralization parameters were established, pathological cases for bone mineralization could be investigated. To investigate these changes, MCaT amd MPO4T,

concentrations were changed to pathological case settings to predict the change in mineralization degree. **Figure 14** shows the change in mineral degree with respect to changes in concentrations of MCaT, where increased concentrations represent hypercalcemic conditions and decreased concentrations represent hypocalcemia. Following aqueous phase and mineral formation dynamics, increased concentrations of Ca^{2+} lead to hyper-mineralization, consistent with cases of hypercalcemia where elevated Ca^{2+} concentrations lead to weak, ductile bones (Fong & Khan, 2012; Leali et al., 2011). This suggests that elevated Ca^{2+} concentrations forms bone with poor mechanical characteristics, specifically mechanical fragility. Contrarily, when Ca^{2+} concentrations are decreased, hypo-mineralization ensues. This outcome is consistent with hypocalcemic conditions due to bones releasing additional calcium required to re-balance the serum concentrations (Blaine, Chonchol, & Levi, 2015). It was also observed that the amount of mineral formed with biological components was much less than what was observed in physicochemical dynamics alone. This is due to the presence of nucleators that limit the amount of mineral formed, where initial nucleator concentration drives the amount of mineral that can be formed.

Figure 14: Mineral formation integrated with biological components of bone mineralization for changes in MCaT. *Matlab code with mineral growth and biology was run simultaneously. Baseline values of MPO4T = 1.28 mM, MHT = 41nM, MCaT =1.21 mM, and V = 1x10^{6}um^3 were utilized. The simulation was run three times, changing the MCaT values for the absolute minimum and maximum concentrations observed in pathology, going from lowest to largest mineral formed, respectively.*

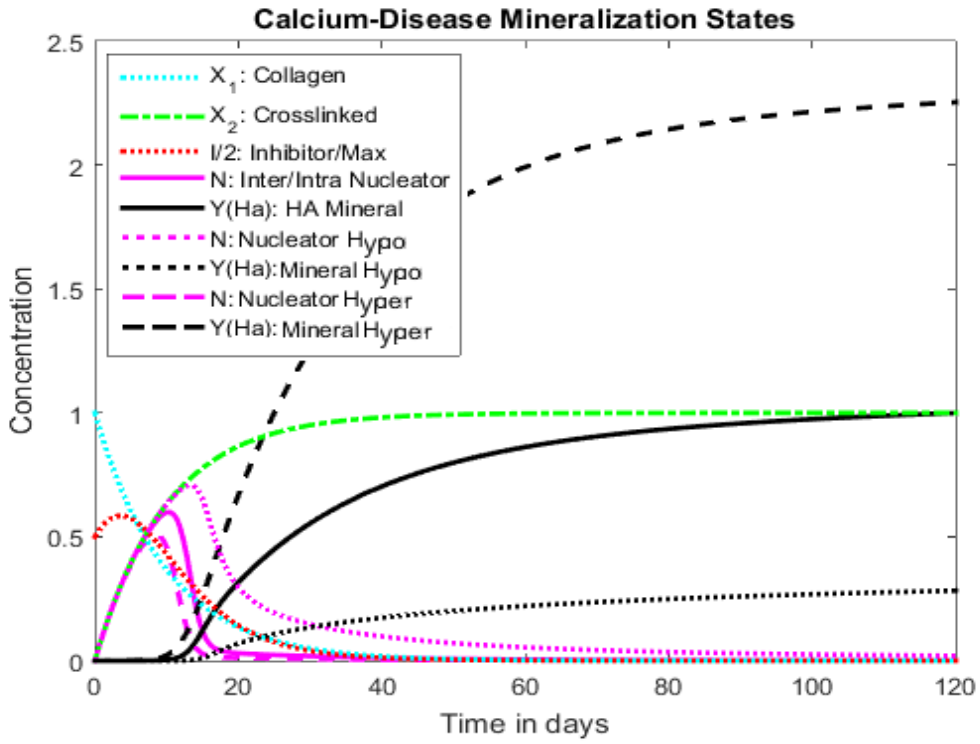

Figure 15 shows the MPO4T concentrations changed to investigate the pathological conditions of hypo and hyper-phosphatemia. Decreasing levels of PO_4^{3-} lead to a decrease in mineral degree, due to lowered concentrations of phosphorous that are required to keep bone healthy. As a result, bone mechanical integrity is compromised, leading to weakened bone structure and mechanical properties (Foster et al., 2008). When PO_4^{3-} concentrations are elevated, mineral degree is increased due to increased calcification, partly in response to the calcium-phosphate product that regulates bone mineralization degree (Cozzolino, Dusso, & Slatopolsky, 2001), which may explain why hyperphosphatemia does not immediately result in decreased mineralization. Mineral amount produced is lower than in cases of hyper-calcemic conditions due to decreased levels of Ca^{2+} and PO_4^{3-} concentrations.

Figure 15: Mineral formation integrated with biological components of bone mineralization for changes in MPO4T. *Matlab code with mineral growth and biology was run simultaneously. Baseline values of MPO4T = 1.28 mM, MHT = 41nM, MCaT =1.21 mM, and V = 1x10^{6}um^3 were utilized. The simulation was run three times, changing the MPO4T values for the absolute*

minimum and maximum concentrations observed in pathology, going from lowest to largest mineral formed, respectively.

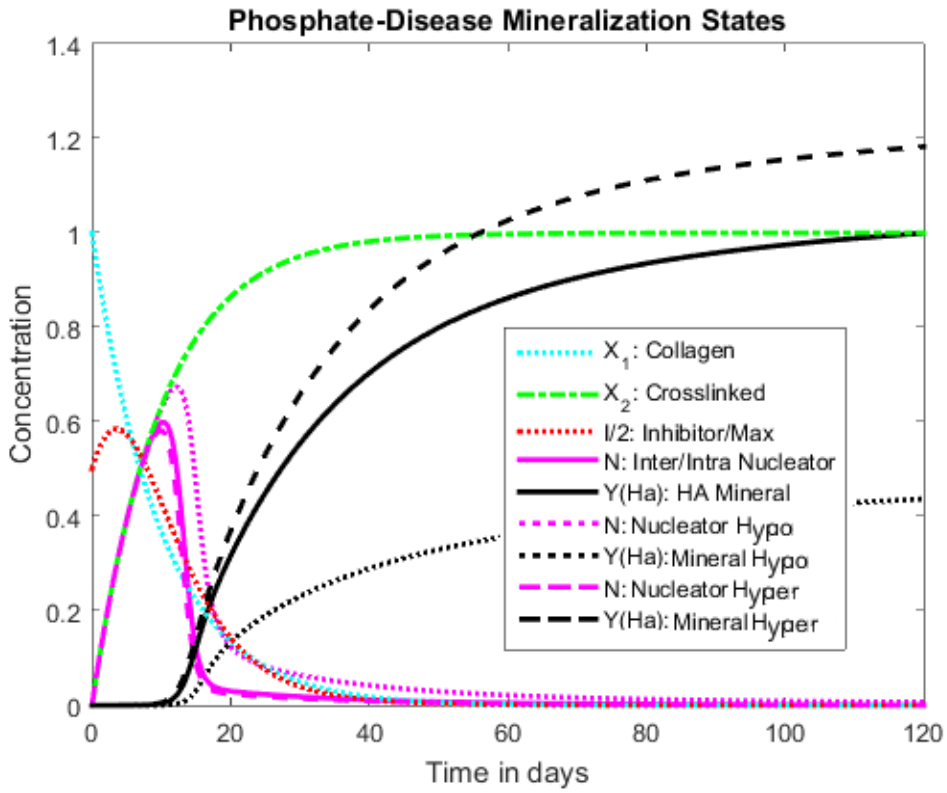

The concentration of MHT was also investigated to predict the changes in mineral degree with respect to the acidity or alkalinity of the bone local microenvironment. Although the initial concentration of MHT is much lower in proportion to the other two elements that form HaP, the general dynamics of mineral degree can be inferred based on chemical laws. An acidic environment (due to an increase in H^+) dissolute HaP and alkaline environments promote Ca^{2+}, PO_4^{3-}, and OH^- ions to produce HaP crystals, which is consistent with experimental and clinical studies performed (Tylavsky, Spence, & Harkness, 2008). However, it should be noted that other mechanisms and physiological processes are present during the exchange of H^+ ions, which should be further investigated to fully understand the role of pH during bone mineralization.

3.4 Conclusion

The current mathematical model proposed is capable of describing the key components of mineralization when individual biological and chemical components are changed to reflect the

state of bone mineralization. With the addition of physicochemical dynamics, the mineral formation component is more precisely predicted through changes in specie concentrations in the local bone microenvironment. To validate the accuracy of physicochemical dynamics in the mathematical model, aqueous phase equilibrium, supersaturation, and chemical mineral formation were investigated and compared with existing literature in chemically precipitated calcium salts. As the stoichiometric coefficients of HaP favour calcium, the mineral degree was proportionally affected by the concentration of calcium available. This was observed when validating the model with bone mineralization diseases, particularly hypo-calcemia and phosphatemia, where significantly decreased concentrations of Ca^{2+} decreased mineral formation. Furthermore, acidosis in bone mineralization suggests mineral dissolution and alkalosis encourages mineral formation, in relation with the increased ion pairing between HaP elements and H^{+} ions. The mathematical model presented can be adapted to predict mineralization in other tissues, such as tooth dentin and enamel, as well as pathological mineralization present in vascular and muscle calcification.

Chapter 4: Discussion and Future Directions

4.1 Discussion

For more than three quarters of a century, the mechanism by which calcium salts precipitate has been heavily disputed in literature (Helt, 1976). The debate is whether nucleation and growth occur simultaneously or whether they are two distinctly different stages of calcium precipitation, as different environmental factors, such as temperature and ionic strength, as well as the substrate which the calcium salt is bound to, all affect the precipitation process. Although both nucleation and growth take thermodynamics into consideration, the difference between using CNT and kinetic theories contrasts between accounting for free energy change of the surface, precipitating nuclei, and bulk of solution, and accounting for the concentration differences between the surface and bulk of solution, respectively. As a result, the kinetic theory for diffusive-reactive processes results in the mass of calcium salt being deposited onto the substrate. When considering bone mineralization as the biological system of interest, HaP formation requires the amount of mass deposited onto the collagen matrix, as nucleators of bone mineralization are accounted for by biological proteins present in the extracellular matrix (Komarova et al., 2015). This results in nucleators forming before calcium salts can be deposited, constituting two distinct processes of calcium precipitation in bone mineralization with crystal growth representing mineral formation.

The mathematical model developed for bone mineralization captures the dynamics of bone mineralization previously observed and includes physicochemical dynamics as part of the mineral formation process. The assumptions of inhibitors suppressing initial mineralization until collagen maturation and nucleators being removed proportionally to the mineral being formed was retained in this model to achieve the dynamics observed. The physicochemical parameters introduced in this model were varied to investigate how mineralization dynamics are affected. Of interest, the initial concentrations MCaT, MPO4T, and MHT, which were included in the formation of mineral, were able to change the lag time and mineralization degree depending on the concentration chosen. To validate the new parameters, the values were compared to other biological systems that included physicochemical kinetics and appropriately applied to the dynamics seen in bone mineralization.

When attempting to equilibrate the system, the equilibrium constants for eight species were varied across the seven studies that reported their values. As equilibrium constants are determined at different ionic strengths, temperature, and adjustment to the specific biological system in question, this may lead to uncertainty in the equilibrium constants (Jawaid & Ingman, 1978). The difference in equilibrium constants is forwarded onto the supersaturation and mineral growth equations, where large differences may change the supersaturation value at the same values of initial concentrations. As most aqueous speciation programs include some sort of standard thermodynamic database, with reaction constants being part of the database, the biological systems using these values are closer to each other; however, these databases contain significant errors and should be investigated further to properly account for speciation calculations (Serkiz, Allison, Michael Perdue, Allen, & Brown, 1996).

A similar problem is observed when investigating the K_{sp} value for HaP, as the values reported are not always consistent. Since the solubility constant is calculated from the equilibrium constants for HaP, the value carries the same errors associated from the previous calculations for speciation calculations. The K_{sp} value for HaP is also affected by the different impurities of HaP, where magnesium, carbonate acid, and other elements may be present in biological systems (Pan & Darvell, 2010). This changes the Ca/P ratio of HaP from the ideal 1.67 and, as a result, affects its solubility dynamics. Further investigation into the type of HaP formed during bone mineralization should be considered to properly account for the solubility of HaP.

Mineral precipitation using Koutsokos' crystal growth equation was applied once HaP was determined to be supersaturated. The precipitation constant (synonymously reported as mass transfer coefficient in some studies) was the experimental constant changed according to the biological system studied. As Koutsokos' crystal growth equation resulted in mineral amount and volume well below the physiological norm, the precipitation constant was adjusted to be around the estimated density of 1200-2000 mg/cm^3 HaP in bone. The previous assumption of not including physical limitations for maximum amount of mineral being formed was now introduced. This accounted for geometric and spatial considerations, where the mineral growth was limited by the amount of ion concentration available in the extracellular reservoir. To date, it is unknown if any other mathematical model incorporates biological components with

physicochemical dynamics to account for volumetric constraints. This provides more accuracy when investigating long-term predictions and allows for subtle changes in volume or ion concentrations that affect the dynamics of mineral formation.

The volumetric constraints changed the overall precipitation dynamics of HaP, where mineral was determined to infinitely form at $1x10^{-6}m^3$ and was limited at volumes less than $1x10^{-12}m^3$. The difference between infinite availability of ions in the extracellular space and limited amounts has implications for current and further experimental studies. As precipitation of any mineral is generally limited by the supply of reagents and the size in which the experiment is conducted, the mathematical predictions more accurately represent the experimental conditions and physiological conditions encountered (Xyla, Mikroyannidis, & Koutsoukos, 1992). It is important to note that the mineral volume produced is six orders of magnitude less than the initial volume and thus does not cut into the original volume. However, these values are dependent upon the reported value for volume of the mineral (Molar mass/mass density), where the mass density is not universally accepted as in other precipitating salts. The vague and poor reporting of the mass density may be due to the impurities present in the type of HaP being precipitated and its associated Ca/P ratio produced, which will affect its material properties.

Once mineral formation dynamics were established, model predictions for biological components integrated with physicochemical dynamics were validated with bone disorders of bone mineralization, such as hyper- and hypo-calcemia/phosphatemia. In cases of hypo-calcemia and phosphatemia, assumed to be observed in osteomalacia, the mineral lag time is increased and the mineral degree decreased due to the low levels of calcium and/or phosphate (Komarova et al., 2015). The current mathematical model correctly predicts this dynamic and can fine tune the amount of calcium or phosphate deficiency that results in a magnitude change of the increased lag time and decreased mineral formed. In cases of hypercalcemia, brittle bone is formed due to hyper-mineralization (increase mineral degree) with lag time being decreased due the rapid use of nucleators (Fong & Khan, 2012; Leali et al., 2011). There are a few dynamics, specifically severe hyperphosphatemia, which the mathematical model struggles to properly predict. The mismatch between elevated levels of phosphate and lowered calcium causes binding of calcium-to-phosphate to eventually drive mineral dissolution, which is not represented in severe

hyperphosphatemic conditions for the current mathematical model. Calcium-to-phosphate binding dynamics should be included to account for this biological phenomenon. Also, total hydrogen concentration at the local bone microenvironment should be investigated to properly predict acidosis and alkalosis bone disease states.

4.2 Future Directions

The mathematical model presented, describing bone mineralization with the integration of physicochemical dynamics, provides a more accurate outlook on the integrated physiological and chemical processes that occur in the bone microenvironment; however, it still presents numerous challenges that can be addressed to further improve the model. Some of these challenges include calcium-phosphate binding dynamics, geometric considerations of HaP, and biological process assumptions that can improve the understanding of bone mineralization dynamics.

Currently, the mathematical model forms HaP mineral with respect to the chemical reactions that are present. The chemical laws of reacting species are followed during mineral growth; however, it is known that proteins and other biological components may disrupt this dynamic. In particular, the binding between calcium and phosphate that forms HaP is influenced by the enzyme alkaline phosphatase (ALP) in bone. ALP is the by-product of osteoblast activity during bone formation and releases PO_4^{3-} from organic compounds to be used in the mineral formation of HaP (Orimo, 2010). Excessive release of PO_4^{3-} from organic compounds due to elevated levels of ALP activity may eventually decrease mineral formation, ultimately leading to dissolution because of the mismatch of free Ca^{2+} ions and PO_4^{3-}. Further investigation into the role of ALP in mineral formation may aid in explaining how mineral dissolution occurs during severely elevated levels of PO_4^{3-}, which may clarify mineral formation of HaP at severe hyper-phosphatemic conditions.

Geometric considerations of HaP crystal precipitation play a role in determining the mineral morphology and the crystalline structure. Several factors affect the geometry of HaP, including changes in temperature, pH, and ion diffusion (Uskoković, 2015). The crystalline structure of HaP may then form as needle, bar, or wires due to the altered local bone microenvironment, which may affect the mechanical properties of bone. It is unknown whether the crystal plane of HaP affects the adsorption profile onto mature collagen during bone mineralization; however, modification in the surface charge, due to changes in pH, attracts certain crystal planes of HaP

that change the crystallization rate and Ca/P ratio (Han et al., 2013). To accurately investigate HaP's crystalline structure and its effect on bone mechanical properties, the geometry of HaP should be considered and can be implemented through investigating crystal-surface contact angles and surface tension (Koutsoukos & Nancollas, 1981).

As the mathematical model tries to recapitulate bone mineralization using a simplistic approach, some of the biological parameters were an ensemble of entities, which were pooled together to represent a single biological process. The inhibitors and nucleators of mineralization are highly complex in nature and were simplified; however, some biological processes could not be properly explained and can be further investigated. For example, the SIBLING protein dentin matrix protein 1 (DMP1) acts as a potent inhibitor within solution; however, once absorbed onto the collagen matrix, DMP1 becomes an active nucleator (Goldberg et al., 1996; He et al., 2005). There are two types of nucleators that are present in bone mineralization, interfibrillar and intrafibrillar, whose mechanisms may be the same or different (Bonucci, 2013). Presently, it is assumed that the two nucleators act the same in mechanism; however, the location of crystal nucleators may affect HaP crystal orientation, size, and shape with respect to the fibril axis, as well as the mechanical properties of bone. As intrafibrillar nucleators are located within the collagen fibrils, the load bearing properties of bone are supported by the crystals deposited in this area as opposed to the mechanical integrity properties on the surface of collagen (Nair, Gautieri, & Buehler, 2014). Therefore, the difference in inhibitor and nucleator concentration and location may change the temporal and spatial dynamics of mineral formation and should be investigated.

4.3 Summary of Findings

The aim of the thesis was to further develop a mathematical model for bone mineralization that would more precisely represent the physicochemical dynamics occurring during HaP precipitation. The focus was to understand how the local balance of ions, that form HaP, affect mineral formation in the presence of healthy and pathological case settings.

Chapter 2 was an overview of existing literature that modelled calcium phosphate precipitation in biological systems. As the primary mechanism of precipitating calcium salts was unclear throughout the modelling or experimental studies originally retrieved, a scoping review was performed to understand all possible mechanisms included in mathematical models of

precipitating calcium salts. The review uncovered three major biological systems that studied calcium precipitation: water research, agricultural sciences, and human biology, with the majority of CPs studied classified as CPPs. Within these three categoreis of biological systems, it was determined that earlier studies focused on nucleation or growth of CPs, while later studies combined these two mechanisms of precipitation. Nucleation was predominantely described by the classical nucleation theory and growth was described by kinetic, with nucleation focusing on the formation of the initial crystal nuclei and growth focusing on the mass deposition of the crystal and later stages of nuclei formation. As the previous model had included biological nucleators for HaP precipitation during bone formation, crystal growth was found to be the predominant mechanism during HaP mass deposition in bone mineralization, with the diffusion-reaction process being chosen for the mathematical model. Since attempts to theoretically describe both biological and physicochemical aspects of the process were rare in the biological systems found within the scoping review, this lead to the updated mathematical model that was updated to include physicochemical dynamics and integrated with the existing biology present to accurately describe bone mineralization.

This lead to the updated mathematical model developed in Chapter 3, which can describe key components of mineralization when individual biological and chemical components are changed to reflect the state of bone mineralization. The addition of physicochemical dynamics, in the form of aqueous phase equilibrium, supersaturation, and mineral formation, revealed insights into the changes of ion concentrations that form HaP at healthy and pathological bone mineralization states. It was found that Ca^{2+} had the strongest influence on HaP formation in purely chemical conditions; however, when coupled with biological components, Ca^{2+} had a suppressed effect on HaP formation due to the presence of biological nucleators. Low concentrations of MCaT and MPO4T lead to hypo-mineralization, where the mineral degree and lag time resembled pathological bone mineralization states, such as hypo-calcemia and hypo-phosphatemia, respectively. High concentrations of MCaT and MPO4T lead to hyper-mineralization of the bone mineral. Finally, acidic and alkaline conditions of bone mineralization were investigated, with acidosis in bone mineralization suggesting mineral dissolution and alkalosis encouraging mineral formation.

Insights into the hypo- or hyper-mineralized states of bone mineralization can uncover the mechanical integrity and quality of the bone mineral being formed with changes to the initial serum concentrations in the body. As such, it is possible to determine the abundance of Ca^{2+} concentration needed to lead to mechanical fragility or how slight of a reduction in PO_4^{3-} is needed to lead to weakened bone structure and mechanical properties. The mathematical model presented with its integrated physicochemical dynamics can be adapted to predict mineralization in other tissues, such as tooth dentin and enamel, as well as pathological mineralization present in vascular and muscle calcification.

References

Abdelkebir, K., Morin-Grognet, S., Gaudiere, F., Coquerel, G., Labat, B., Atmani, H., & Ladam, G. (2012). Biomimetic layer-by-layer templates for calcium phosphate biomineralization. *Acta Biomaterialia, 8*(9), 3419-3428. doi: 10.1016/j.actbio.2012.05.035

Anderson, H. C. (2003). Matrix vesicles and calcification. *Current Rheumatology Reports, 5*(3), 222-226.

Appelman-Dijkstra, N. M., & Papapoulos, S. E. (2015). Modulating Bone Resorption and Bone Formation in Opposite Directions in the Treatment of Postmenopausal Osteoporosis. *Drugs, 75*(10), 1049-1058. doi: 10.1007/s40265-015-0417-7

Arnett, T. R. (2008). Extracellular pH Regulates Bone Cell Function. *The Journal of Nutrition, 138*(2), 415S-418S. doi: 10.1093/jn/138.2.415S

Atkins, G., et al. (2012). Sclerostin is a Locally Acting Regulator of Late-Osteoblast/Preosteocyte Differentation and Regulates Mineralization Through a MEPE-ASARM-Dependent Mechanism. *Journal of Bone and Mineral Research, 26*(7), 1425-1436. doi: 10.1002/jbmr.345

Barat, R., Montoya, T., Seco, A., & Ferrer, J. (2011). Modelling biological and chemically induced precipitation of calcium phosphate in enhanced biological phosphorus removal systems. *Water Res, 45*(12), 3744-3752. doi: 10.1016/j.watres.2011.04.028

Berthoud, A. (1912). Théorie de la formation des faces d'un cristal1. *J. Chim. Phys., 10*, 624-635.

Blaine, J., Chonchol, M., & Levi, M. (2015). Renal Control of Calcium, Phosphate, and Magnesium Homeostasis. *Clinical Journal of the American Society of Nephrology : CJASN, 10*(7), 1257-1272. doi: 10.2215/CJN.09750913

Blair, H. C., Larrouture, Q. C., Li, Y. N., Lin, H., Beer-Stoltz, D., Liu, L., . . . Nelson, D. J. (2017). Osteoblast Differentiation and Bone Matrix Formation In Vivo and In Vitro. *Tissue Engineering Part B-Reviews, 23*(3), 268-+. doi: 10.1089/ten.teb.2016.0454

Boistelle, R., & Lopez-Valero, I. (1990). Growth units and nucleation: The case of calcium phosphates. *CRYS</cja:jid> Journal of Crystal Growth, 102*(3), 609-617.

Bonucci, E. (2013). The mineralization of bone and its analogies with other hard tissues *Advanced Topics on Crystal Growth*: InTech.

Boskey, A. L. (1996). Matrix proteins and mineralization: An overview. *Connective Tissue Research, 35*(1-4), 357-363. doi: 10.3109/03008209609029212

Boyce, B. F., & Xing, L. (2008). Functions of RANKL/RANK/OPG in bone modeling and remodeling. *Archives of Biochemistry and Biophysics, 473*(2), 139-146.

Brar, T., France, P., & Smirniotis, P. G. (2001). Heterogeneous versus Homogeneous Nucleation and Growth of Zeolite A. *The Journal of Physical Chemistry B, 105*(23), 5383-5390. doi: 10.1021/jp003012f

Burghardt, A. J., Kazakia, G. J., Laib, A., & Majumdar, S. (2008). Quantitative assessment of bone tissue mineralization with polychromatic micro-computed tomography. *Calcified Tissue International, 83*(2), 129-138. doi: 10.1007/s00223-008-9158-x

Chen, L., Jacquet, R., Lowder, E., & Landis, W. (2014). Refinement of collagen-mineral interaction: A possible role for osteocalcin in apatite crystal nucleation, growth and development. *Bone*, *71*, 7-16.

Christian, J. W. (1975). *The Theory of Transformations in Metals and Alloys* (1st ed.). University of Oxford, UK: Pergamon.

Christiansen, D. L., Huang, E. K., & Silver, F. H. (2000). Assembly of type I collagen: fusion of fibril subunits and the influence of fibril diameter on mechanical properties. *Matrix Biology, 19*(5), 409-420. doi: https://doi.org/10.1016/S0945-053X(00)00089-5

Clarke, B. (2008). Normal Bone Anatomy and Physiology. *Clinical Journal of the American Society of Nephrology : CJASN, 3*(Suppl 3), S131-S139. doi: 10.2215/CJN.04151206

Cozzolino, M., Dusso, A. S., & Slatopolsky, E. (2001). Role of calcium-phosphate product and bone-associated proteins on vascular calcification in renal failure. *Journal of the American Society of Nephrology, 12*(11), 2511-2516.

D., M. M., & Antonio, N. (1996). Osteopontin deposition in remodeling bone: An osteoblast mediated event. *Journal of Bone and Mineral Research, 11*(6), 873-874. doi: doi:10.1002/jbmr.5650110620

Dallas, S. L., Prideaux, M., & Bonewald, L. F. (2013). The osteocyte: an endocrine cell… and more. *Endocrine reviews, 34*(5), 658-690.

Davies, C. (1962). *Ion Association*. London: Butterworths.

De Yoreo, J. J. (2003). Principles of Crystal Nucleation and Growth. *Reviews in Mineralogy and Geochemistry Reviews in Mineralogy and Geochemistry, 54*(1), 57-93.

Debye, P., & Hückel, E. (1923). Zur Theorie der Elektrolyte. I. Gefrierpunktserniedrigung und verwandte Erscheinungen. The theory of electrolytes. I. Lowering of freezing point and

related phenomena. *Physikalische Zeitschrift, 24*, 185-206. doi: citeulike-article-id:9751523

E.C. Moreno, T. M. G., W.E. Brown. (1968). Preparation and Solubility of Hydroxyapatite. *Journal of Research of the National Bureau of Standards - A. Physics and Chemistry, 72A*(6), 773-782.

Finkel, A. (1990). *Confronting Uncertainty in Risk Management: A Guide for Decision Makers*.

Florencio-Silva, R., Sasso, G. R. d. S., Sasso-Cerri, E., Simões, M. J., & Cerri, P. S. (2015). Biology of Bone Tissue: Structure, Function, and Factors That Influence Bone Cells. *BioMed Research International, 2015*, 421746. doi: 10.1155/2015/421746

Fong, J., & Khan, A. (2012). Hypocalcemia: Updates in diagnosis and management for primary care. *Canadian Family Physician, 58*(2), 158-162.

Foster, B. L., Tompkins, K. A., Rutherford, R. B., Zhang, H., Chu, E. Y., Fong, H., & Somerman, M. J. (2008). Phosphate: Known and potential roles during development and regeneration of teeth and supporting structures. *Birth defects research. Part C, Embryo today : reviews, 84*(4), 281-314. doi: 10.1002/bdrc.20136

Garnero, P. (2012). The contribution of collagen crosslinks to bone strength. *BoneKEy Reports, 1*, 182. doi: 10.1038/bonekey.2012.182

George, A., & Hao, J. J. (2005). Role of phosphophoryn in dentin mineralization. *Cells Tissues Organs, 181*(3-4), 232-240. doi: 10.1159/000091384

Gibbs, J. W. (1878). On the Equilibrium of Heterogeneous Substances. *American journal of science, 96*, 441-458.

Glorieux, F., et al. (2002). Osteogenesis imperfecta type VI: a form of brittle bone disease with a mineralization defect. *Journal of Bone Mineral Research, 17*(1), 30-38.

Goldberg, H. A., Warner, K. J., Stillman, M. J., & Hunter, G. K. (1996). Determination of the hydroxyapatite-nucleating region of bone sialoprotein. *Connective Tissue Research, 35*(1-4), 385-392. doi: 10.3109/03008209609029216

H. Drake, F., W. Pierce, G., & T. Dow, M. (1930). *Measurement of the Dielectric Constant and Index of Refraction of Water and Aqueous Solutions of KCl at High Frequencies* (Vol. 35).

Han, G. S., Lee, S., Kim, D. W., Kim, D. H., Noh, J. H., Park, J. H., . . . Jung, H. S. (2013). A Simple Method To Control Morphology of Hydroxyapatite Nano- and Microcrystals by

Altering Phase Transition Route. *Crystal Growth & Design, 13*(8), 3414-3418. doi: 10.1021/cg400308a

Hanrahan, G. (2010). Modelling of pollutants in complex environmental systems. Volume 2 Volume 2.

Hassanali, L., Wong, F. S., Lynch, R. J. M., & Anderson, P. (2017). A Novel Kinetic Method to Measure Apparent Solubility Product of Bulk Human Enamel. *Frontiers in Physiology, 8*, 714. doi: 10.3389/fphys.2017.00714

He, G., Gajjeraman, S., Schultz, D., Cookson, D., Qin, C. L., Butler, W. T., . . . George, A. (2005). Spatially and temporally controlled biomineralization is facilitated by interaction between self-assembled dentin matrix protein 1 and calcium phosphate nuclei in solution. *Biochemistry, 44*(49), 16140-16148. doi: 10.1021/bi0510451

Helgeson, H. C. (1969). Thermodynamics of hydrothermal systems at elevated temperatures and pressures. *American journal of science, 267*(7), 729-804.

Helt, J. E. (1976). Effects of supersaturation and temperature on nucleation and crystal growth in a MSMPR crystallizer. *Retrospective Theses and Dissertations*, 6213.

Hunter, G. K., & Goldberg, H. A. (1993). Nucleation of hydroxyapatite by bone sialoprotein. *Proceedings of the National Academy of Sciences of the United States of America, 90*(18), 8562-8565.

Islam, M. Z., Shamim, A. A., Kemi, V., Nevanlinna, A., Akhtaruzzaman, M., Laaksonen, M., . . . Lamberg-Allardt, C. (2008). Vitamin D deficiency and low bone status in adult female garment factory workers in Bangladesh. *British Journal of Nutrition, 99*(6), 1322-1329.

Isopescu, R., Mateescu, C., Mihai, M., & Dabija, G. (2010). The effects of organic additives on induction time and characteristics of precipitated calcium carbonate. *Chemical Engineering Research and Design, 88*(11), 1450-1454. doi: 10.1016/j.cherd.2009.10.002

Jawaid, M., & Ingman, F. (1978). Ion-pair extraction of Na+, K+ and Ca2+ with some organic counter-ions and dicyclohexyl-18-crown-6 as adduct-forming reagent. *Talanta, 25*(2), 91-95. doi: https://doi.org/10.1016/0039-9140(78)80039-3

Kaartinen, M. T., El-Maadawy, S., Rasanen, N. H., & McKee, M. D. (2002). Tissue transglutaminase and its substrates in bone. *Journal of Bone & Mineral Research, 17*(12), 2161-2173. doi: 10.1359/jbmr.2002.17.12.2161

Kalikmanov, V. I. (2013). Nucleation theory.

Kapinas, K., & Delany, A. (2011). *MicroRNA biogenesis and regulation of bone remodeling* (Vol. 13).

Karthika, S., Radhakrishnan, T. K., & Kalaichelvi, P. (2016). A Review of Classical and Nonclassical Nucleation Theories. *Crystal Growth & Design, 16*(11), 6663-6681. doi: 10.1021/acs.cgd.6b00794

Knott, L., & Bailey, A. J. (1998). Collagen cross-links in mineralizing tissues: A review of their chemistry, function, and clinical relevance. *BON</cja:jid> Bone, 22*(3), 181-187.

Kobayashi, S., Takahashi, H. E., Ito, A., Saito, N., Nawata, M., Horiuchi, H., . . . Takaoka, K. (2003). Trabecular minimodeling in human iliac bone. *Bone, 32*(2), 163-169.

Komarova, S., Safranek, L., Gopalakrishnan, J., Ou, M.-j., Mckee, M., Murshed, M., . . . Zuhr, E. (2015). Mathematical model for bone mineralization. *Frontiers in Cell and Developmental Biology, 3*(51). doi: 10.3389/fcell.2015.00051

Koutsoukos, P. G., & Nancollas, G. H. (1981). Crystal growth of calcium phosphates - epitaxial considerations. *Journal of Crystal Growth, 53*(1), 10-19. doi: http://dx.doi.org/10.1016/0022-0248(81)90051-8

Leali, P. T., Muresu, F., Melis, A., Ruggiu, A., Zachos, A., & Doria, C. (2011). Skeletal fragility definition. *Clinical Cases in Mineral and Bone Metabolism, 8*(2), 11-13.

Liu, X. Y. (1999). A new kinetic model for three-dimensional heterogeneous nucleation. *The Journal of Chemical Physics The Journal of Chemical Physics, 111*(4), 1628-1635.

Liu, X. Y. (2001). Influence of nucleation nature on Ca mineral/substrate structural synergy and implications for biomineralization in microgravity. *The Journal of Chemical Physics The Journal of Chemical Physics, 115*(21), 9970-9974.

Liu, X. Y. (2001). Interfacial process of nucleation and molecular nucleation templator. *Appl. Phys. Lett. Applied Physics Letters, 79*(1), 39-41.

Liu, Y., Wu, W., Sethuraman, G., & Nancollas, G. H. (1997). Intergrowth of calcium phosphates: an interfacial energy approach. *CRYS</cja:jid> Journal of Crystal Growth, 174*(1), 386-392.

Locklin, R. M., Oreffo, R. O., & Triffitt, J. T. (1999). Effects of TGFbeta and bFGF on the differentiation of human bone marrow stromal fibroblasts. *Cell Biology International, 23*(3), 185-194. doi: 10.1006/cbir.1998.0338

Lu, X., & Leng, Y. (2005). Theoretical analysis of calcium phosphate precipitation in simulated body fluid. *JBMT Biomaterials, 26*(10), 1097-1108.

M. Serkiz, S., Allison, J., Michael Perdue, E., E. Allen, H., & S. Brown, D. (1996). *Correcting errors in the thermodynamic database for the equilibrium speciation model MINTEQA2* (Vol. 30).

Manov, G. G., Bates, R. G., Hamer, W. J., & Acree, S. F. (1943). Values of the Constants in the Debye—Hückel Equation for Activity Coefficients1. *Journal of the American Chemical Society, 65*(9), 1765-1767. doi: 10.1021/ja01249a028

Margolis, H. C., Kwak, S.-Y., & Yamazaki, H. (2014). Role of mineralization inhibitors in the regulation of hard tissue biomineralization: relevance to initial enamel formation and maturation. *Frontiers in Physiology, 5*, 339. doi: 10.3389/fphys.2014.00339

Martin, B. (1994). Mathematical model for the mineralization of bone. *J Orthop Res, 12*(3), 375-383. doi: 10.1002/jor.1100120310

Mescher, A. (2016). *Junqueira's Basic Histology Text & Atlas (14th ed.)*. USA: McGraw-Hill Education.

Meyer, J., & Reddi, A. (1985). Changes in pyrophosphatase activity during the de novo mineralization associated with cartilage and bone formation. *Archives of biochemistry and biophysics, 242*(2), 532-539.

Moe, S. M. (2008). Disorders Involving Calcium, Phosphorus, and Magnesium. *Primary care, 35*(2), 215-vi. doi: 10.1016/j.pop.2008.01.007

Mohan, C. (2006). Buffers - A guide for the preparation and use of buffers in biological systems. In Calbiochem (Ed.). San Diego, USA: EMD Biosciences, Inc.

Montastruc, L., Azzaro-Pantel, C., Cabassud, M., & Biscans, B. (2002). *Calcium Phosphate Precipitation in a Pellet Reactor*.

Montastruc, L., Azzaro-Pantel, C., Davin, A., Pibouleau, L., Cabassud, M., & Domenech, S. (2003). A hybrid optimization technique for improvement of P-recovery in a pellet reactor. In A. Kraslawski & I. Turunen (Eds.), *European Symposium on Computer Aided Process Engineering - 13* (Vol. 14, pp. 779-784).

Mullin, J. W. (2001). *Crystallization* (4th ed.). University College London (Emeritus): Butterworth-Heinemann.

Mullin, J. W. (2014). Crystallization.

Murshed, M., & McKee, M. D. (2010). Molecular determinants of extracellular matrix mineralization in bone and blood vessels. *Current Opinion in Nephrology & Hypertension, 19*(4), 359-365. doi: 10.1097/MNH.0b013e3283393a2b

Musvoto, E. V., Wentzel, M. C., Loewenthal, R. E., & Ekama, G. A. (2000). Integrated chemical-physical processes modelling—I. Development of a kinetic-based model for mixed weak acid/base systems. *WR</cja:jid> Water Research, 34*(6), 1857-1867.

Nair, A. K., Gautieri, A., & Buehler, M. J. (2014). Role of intrafibrillar collagen mineralization in defining the compressive properties of nascent bone. *Biomacromolecules, 15*(7), 2494-2500. doi: 10.1021/bm5003416

Nancollas, G. H., & Koutsoukos, P. G. (1980). Calcium phosphate nucleation and growth in solution. *Progress in Crystal Growth and Characterization Progress in Crystal Growth and Characterization, 3*(1), 77-102.

Nielsen, A. E. (1984). Electrolyte crystal growth mechanisms. *CRYS</cja:jid> Journal of Crystal Growth, 67*(2), 289-310.

Noyes, A. A., & Whitney, W. R. (1897). THE RATE OF SOLUTION OF SOLID SUBSTANCES IN THEIR OWN SOLUTIONS. *J. Am. Chem. Soc. Journal of the American Chemical Society, 19*(12), 930-934.

Obermeyer, Z., Samra, J. K., & Mullainathan, S. (2017). Individual differences in normal body temperature: longitudinal big data analysis of patient records. *BMJ, 359*. doi: 10.1136/bmj.j5468

Oldberg, A., Franzen, A., & Heinegard, D. (1988). The primary structure of a cell-binding bone sialoprotein. *Journal of Biological Chemistry, 263*(36), 19430-19432.

Oliveira, C., Ferreira, A., & Rocha, F. (2007). Dicalcium Phosphate Dihydrate Precipitation:Characterization and Crystal Growth. *CHERD Chemical Engineering Research and Design, 85*(12), 1655-1661.

Oliveira, C., Georgieva, P., Rocha, F., Ferreira, A., & de Azevedo, S. F. (2007). Dynamical model of brushite precipitation. *Journal of Crystal Growth, 305*(1), 201-210. doi: 10.1016/j.jcrysgro.2007.04.016

Olson, G., Chung-Shuan Inst. of, S., & Tech. (2000). A model for nonclassical nucleation of solid-solid structural phase transformations. *Metallurgical and Materials Transactions. A, Physical Metallurgy and Materials Science, 31*(5), 1321-1332.

Olszta, M. J., Cheng, X. G., Jee, S. S., Kumar, R., Kim, Y. Y., Kaufman, M. J., . . . Gower, L. B. (2007). Bone structure and formation: A new perspective. *Materials Science & Engineering R-Reports, 58*(3-5), 77-116. doi: 10.1016/j.mser.2007.05.001

Orimo, H. (2010). The mechanism of mineralization and the role of alkaline phosphatase in health and disease. *J Nippon Med Sch, 77*(1), 4-12.

Ostwald, W. (1900). Über die vermeintliche Isomerie des roten und gelben Quecksilbersoxyds und die Oberflächenspannung fester Körper. *Zeitschrift für physikalische Chemie, 34*, 495-503.

Ouzzani, M., Hammady, H., Fedorowicz, Z., & Elmagarmid, A. (2016). Rayyan-a web and mobile app for systematic reviews. *Syst Rev, 5*(1), 210. doi: 10.1186/s13643-016-0384-4

Palmer, L. C., Newcomb, C. J., Kaltz, S. R., Spoerke, E. D., & Stupp, S. I. (2008). Biomimetic Systems for Hydroxyapatite Mineralization Inspired By Bone and Enamel. *Chemical reviews, 108*(11), 4754-4783. doi: 10.1021/cr8004422

Pan, H., & Darvell, B. (2010). *Effect of Carbonate on Hydroxyapatite Solubility* (Vol. 10).

Petersson, U., Somogyi, E., Reinholt, F. P., Karlsson, T., Sugars, R. V., & Wendel, M. (2004). Nucleobindin is produced by bone cells and secreted into the osteoid, with potential role as a modulator of matrix maturation. *Bone, 34*(6), 949-960. doi: 10.1016/j.bone.2004.01.019

Pitzer, K. S. (1973). Thermodynamics of electrolytes. I. Theoretical basis and general equations. *The Journal of physical chemistry, 77*(2), 268-277. doi: 10.1021/j100621a026

Poduri, R., & Chen, L. Q. (1996). Non-classical nucleation theory of ordered intermetallic precipitates—application to the Al□Li alloy. *Acta Materialia, 44*(10), 4253-4259. doi: https://doi.org/10.1016/S1359-6454(96)00037-7

Raisz, L. G., & Rodan, G. A. (1998). Embryology and cellular biology of bone *Metabolic Bone Disease and Clinically Related Disorders (Third Edition)* (pp. 1-22): Elsevier.

RE Loewenthal, G. E., GvR Marais. (1989, January 1st, 1989). *Mixed weak acid/base systems Part 1 — Mixture characterisation*. [Water SA Manuscript]. (496, 15 No. 1). South Africa.

Recillas, S., Rodriguez-Lugo, V., Montero, M. L., Viquez-Cano, S., Hernandez, L., & Castano, V. M. (2012). Studies on the precipitation behavior of calcium phosphate solutions. *Journal of Ceramic Processing Research, 13*(1), 5-10.

Reuss-Borst, M. A. (2014). [Metabolic bone disease osteomalacia]. *Zeitschrift fur Rheumatologie, 73*(4), 316-322.

Rice, G., Barber, A., O'Connor, A., Stevens, G., & Kentish, S. (2010). A theoretical and experimental analysis of calcium speciation and precipitation in dairy ultrafiltration permeate. *International Dairy Journal, 20*(10), 694-706. doi: 10.1016/j.idairyj.2010.03.004

Robling, A. G., Castillo, A. B., & Turner, C. H. (2006). BIOMECHANICAL AND MOLECULAR REGULATION OF BONE REMODELING. *Annual Review of Biomedical Engineering, 8*(1), 455-498. doi: 10.1146/annurev.bioeng.8.061505.095721

Roodman, G. D. (1999). Cell biology of the osteoclast. *Experimental Hematology, 27*(8), 1229-1241.

Roschger, P., Paschalis, E. P., Fratzl, P., & Klaushofer, K. (2008). Bone mineralization density distribution in health and disease. *Bone, 42*(3), 456-466. doi: 10.1016/j.bone.2007.10.021

Schaffler, M. B., Cheung, W.-Y., Majeska, R., & Kennedy, O. (2014). Osteocytes: Master Orchestrators of Bone. *Calcified Tissue International, 94*(1), 5-24. doi: 10.1007/s00223-013-9790-y

Sebastián-Serrano, Á., de Diego-García, L., Martínez-Frailes, C., Ávila, J., Zimmermann, H., Millán, J. L., . . . Díaz-Hernández, M. (2015). Tissue-nonspecific Alkaline Phosphatase Regulates Purinergic Transmission in the Central Nervous System During Development and Disease. *Computational and Structural Biotechnology Journal, 13*, 95-100. doi: 10.1016/j.csbj.2014.12.004

Sekhon, K., Kazakia, G. J., Burghardt, A. J., Hermannsson, B., & Majumdar, S. (2009). Accuracy of volumetric bone mineral density measurement in high-resolution peripheral quantitative computed tomography. *Bone, 45*(3), 473-479. doi: 10.1016/j.bone.2009.05.023

Siddiqui, J. A., & Partridge, N. C. (2016). Physiological Bone Remodeling: Systemic Regulation and Growth Factor Involvement. *Physiology, 31*(3), 233-245. doi: 10.1152/physiol.00061.2014

Silver, I. A., Murrills, R. J., & Etherington, D. J. (1988). Microelectrode studies on the acid microenvironment beneath adherent macrophages and osteoclasts. *Experimental Cell Research, 175*(2), 266-276.

Söhnel, O., & Mullin, J. W. (1988). Interpretation of crystallization induction periods. *YJCIS</cja:jid> Journal of Colloid And Interface Science, 123*(1), 43-50.

Solomon, T. (2001). The Definition and Unit of Ionic Strength. *J. Chem. Educ. Journal of Chemical Education, 78*(12), 1691.

Szilágyi, B., Muntean, N., Barabás, R., Ponta, O., & Lakatos, B. G. (2015). Reaction precipitation of amorphous calcium phosphate: Population balance modelling and kinetics. *CHERD Chemical Engineering Research and Design, 93*, 278-286.

Tylavsky, F. A., Spence, L. A., & Harkness, L. (2008). The Importance of Calcium, Potassium, and Acid-Base Homeostasis in Bone Health and Osteoporosis Prevention. *The Journal of Nutrition, 138*(1), 164S-165S. doi: 10.1093/jn/138.1.164S

Uskoković, V. (2015). The Role of Hydroxyl Channel in Defining Selected Physicochemical Peculiarities Exhibited by Hydroxyapatite. *Rsc Advances, 5*, 36614-36633. doi: 10.1039/C4RA17180B

Volmer, M. W., A. (1926). Keimbildung in übersättigten Gebilden. *Zeitschrift für physikalische Chemie, 119*, 277-301.

Wang, K. F., Leng, Y., Lu, X., Ren, F. Z., Ge, X., & Ding, Y. H. (2012). Theoretical analysis of protein effects on calcium phosphate precipitation in simulated body fluid. *Crystengcomm, 14*(18), 5870-5878. doi: 10.1039/c2ce25216c

Wang, L., & Nancollas, G. H. (2008). Calcium orthophosphates: crystallization and dissolution. *Chemical reviews, 108*(11), 4628-4669.

Wang, L. J., Guan, X. Y., Tang, R. K., Hoyer, J. R., Wierzbicki, A., De Yoreo, J. J., & Nancollas, G. H. (2008). Phosphorylation of osteopontin is required for inhibition of calcium oxalate crystallization. *Journal of Physical Chemistry B, 112*(30), 9151-9157. doi: 10.1021/jp804282u

Wang, L. J., Ruiz-Agudo, E., Putnis, C. V., Menneken, M., & Putnis, A. (2012). Kinetics of Calcium Phosphate Nucleation and Growth on Calcite: Implications for Predicting the Fate of Dissolved Phosphate Species in Alkaline Soils. *Environmental Science & Technology, 46*(2), 834-842. doi: 10.1021/es202924f

Wong, A. T. C., & Czernuszka, J. T. (1993). Transformation behaviour of calcium phosphate 1. Theory and modelling. *COLSUA</cja:jid> Colloids and Surfaces A: Physicochemical and Engineering Aspects, 78*, 245-253.

Wyman, J. (1930). Measurements of the Dielectric Constants of Conducting Media. *Physical Review, 35*(6), 623-634.

Xie, Y., Liu, X., Chu, P. K., & Ding, C. (2006). Nucleation and growth of calcium-phosphate on Ca-implanted titanium surface. *SUSC Surface Science, 600*(3), 651-656.

Xyla, A. G., Mikroyannidis, J., & Koutsoukos, P. G. (1992). The inhibition of calcium carbonate precipitation in aqueous media by organophosphorus compounds. *Journal of Colloid and Interface Science, 153*(2), 537-551. doi: https://doi.org/10.1016/0021-9797(92)90344-L

Yamamoto, H., & Sakae, T. (1987). Brushite in fibrous dysplasia of the jaw bone. *Acta Pathol Jpn, 37*(10), 1699-1705.

Yoshiko, Y., Candeliere, G. A., Maeda, N., & Aubin, J. E. (2007). Osteoblast autonomous Pi regulation via Pit1 plays a role in bone mineralization. *Molecular and cellular biology, 27*(12), 4465-4474.

Appendix A: Variables and Parameters

A	Activity coefficient constant
a_{ij}	Stoichiometric coefficient
B	Debye-Huckel parameter
B_{dot}	B-dot parameter
C	Concentration [M]
c_i	Solute concentration in solution [M]
c^*	Equilibrium concentration [M]
D	Dielectric constant
$e+$	Charge of positively charged ions
$e-$	Charge of negatively charged ions
F	Probability factor (Percent)
g	Order of overall crystal growth processes
ΔG	Overall free energy cost of nucleus [kJ/mol]
ΔG_{Hetero}	Heterogenous free energy cost [kJ/mol]
ΔG_{Homo}	Homogenous free energy cost [kJ/mol]
ΔG_s	Interfacial free energy cost [kJ/mol]
ΔG_v	Bulk solution free energy cost [kJ/mol]
h	Height of nuclei forming [m]
I	Ionic strength [mol/kg]
I_{Af}	Newly formed acidic ion concentration [M]
I_{Ao}	Initial concentration of acidic ion [M]
I_{Bf}	Newly formed basic ion concentration [M]

I_{Bo} Initial concentration of basic ion [M]

I_x Inhibitor concentration

k Boltzmann constant

k_1 Collagen assembly [day^{-1}]

k_2 Number of nucleators per collagen molecule

K Reaction kinetic factor

K_c Precipitation constant

k_d Mass transfer coefficient (diffusion) [m/s]

K_G Probability coefficient

K_i Apparent equilibrium constant

k_m General mass transfer coefficient [m/s]

K_p Apparent equilibrium constant

$K_{p'}$ Ratio of reverse and forward reactions

k_r Mass transfer coefficient [m/s]

K_{sp} Solubility constant [$M^{StoichiometricTotal}$]

K_{Xf} Equilibrium constant - forward reaction rate for specie X

K_{Xr} Equilibrium constant reverse reaction rate for specie X

L_{SA} Surface area of the crystal [m^2]

M_T Total mass of j^{th} component [kg]

N Nucleation rate [nuclei/m^3/s]

N_B Number of nucleators

N_c Number of components considered

N_{sp} Number of species considered

Q Effective concentration

Q_T Effective concentration of all components

r Radius of nuclei forming [m]

r_1 Degradation of inhibitors [day^{-1}]

r_2 Use of nucleators by mineralized bone [mol^{-1}]

S Supersaturation [mol/dm^3]

s Total number of growth sites available

T_K Temperature [^0K]

T_C Temperature [^0C]

T_X Total concentration of X specie [M]

t Time [s]

v Volume of nuclei [m^3]

v_1 Production of inhibitors by osteoblasts [day^{-1}]

w Sum of cationic and anionic species

$w+$ Total number of cationic species

$w-$ Total number of anionic species

X_i Activity of species

x_1 Naïve collagen matrix [molecules/μm^3]

x_2 Assembled collagen matrix [molecules/μm^3]

y Amount of HaP formed [g]

z	Charge of ion
α	Diameter of the species [m]
β_n	Balanced equation value for ‘n’ ion
γ_i	Activity coefficient
ε	Relative dielectric constant for the solution
η	Crystallization rate modifier
λ_{cl}	Interfacial free energy constant (crystal-liquid)
λ_{sc}	Interfacial free energy constant (surface-crystal)
λ_{sl}	Interfacial free energy constant (surface-liquid)
Φ	Phase transformation fraction (Percent)
Ψ	Crystal growth [mol/m^3/s]

Appendix B: Relevant tables included in parameter estimation and uncertainty

Table S1: Parameter variability in equilibrium constants

Study	HaP Ksp (M^9)	H_2O (K values)*	$CaOH^+$	$CaPO_4^-$	HPO_4^{2-}	$H_2PO_4^-$	H_3PO_4	$CaHPO_4$	$CaH_2PO_4^+$
[Gregory 1991]	$2.79\cdot10^{-59}$	$1.01\cdot10^{-14}$	20	$2.9\cdot10^{7}$	$4.52\cdot10^{-13}$	$6.31\cdot10^{-8}$	$7.11\cdot10^{-3}$	265	8.45
[Sbarciog 2016]	N/A	$1.004\cdot10^{-14}$	$3.981\cdot10^{-2}$	$3.475\cdot10^{-7}$	$4.508\cdot10^{-13}$	$6.21\cdot10^{-8}$	$7.129\cdot10^{-3}$	$1.823\cdot10^{-3}$	$3.9\cdot10^{-2}$
[Tadayyon 2003]	N/A	$1.007\cdot10^{-14}$	19.952	$2.511\cdot10^{6}$	$4.468\cdot10^{-13}$	$1.581\cdot10^{7}$	$7.11\cdot10^{-3}$	549.54	25.119
[Udert 2003]	$3.162\cdot10^{-58}$	N/A	N/A	N/A	$4.667\cdot10^{-13}$	$6.17\cdot10^{-8}$	N/A	$3.236\cdot10^{-5}$	25.7
[Dupraz 2009]	N/A	$1.462\cdot10^{-14}$	$2.46\cdot10^{-13}$	$1.375\cdot10^{-6}$	$1.916\cdot10^{12}$	$1.565\cdot10^{7}$	$2.44\cdot10^{9}$	549.54	25.12
[Lioliou 2007]	N/A	$1.007\cdot10^{-14}$	0.00513	N/A	N/A	N/A	N/A	N/A	N/A
[Lin 2006]	$10^{-3.421}$	N/A	$2.01\cdot10^{-13}$	$2.88\cdot10^{6}$	$2.37\cdot10^{12}$	$3.95\cdot10^{19}$	$5.26\cdot10^{21}$	$1.084\cdot10^{15}$	N/A
[Musvoto 2000]	N/A	$1\cdot10^{-14}$	23.4423	$2.884\cdot10^{6}$	$9.484\cdot10^{-13}$	$4.274\cdot10^{-7}$	$2.62\cdot10^{-3}$	537.032	25.704
[Barat 2011]	N/A	$1.007\cdot10^{-14}$	-12.697	$2.88\cdot10^{6}$	$2.37\cdot10^{12}$	$3.95\cdot10^{19}$	$5.26\cdot10^{21}$	$1.084\cdot10^{15}$	$8.38\cdot10^{20}$
[Christoffersen 1992]	$5.49\cdot10^{-118}$ (M^{118})	$2.400\cdot10^{-14}$	N/A	$3.02\cdot10^{6}$	$6.76\cdot10^{-13}$	$6.61\cdot10^{-8}$	$6.16\cdot10^{-3}$	380	4.5
[Gebrehiwet 2014]	$8.42\cdot10^{-4}$	$1.02\cdot10^{-14}$	$1.42\cdot10^{-13}$	N/A	$4.79\cdot10^{-13}$	$1.66\cdot10^{7}$	$2.323\cdot10^{9}$	549.54	N/A
[Dalas 2006]	N/A	$1\cdot10^{-14}$	N/A	N/A	N/A	N/A	N/A	N/A	N/A
[Schmidt 1987]	N/A	$1.01\cdot10^{-14}$	20	$2.88\cdot10^{6}$	$4.05\cdot10^{-13}$	$3.52\cdot10^{-8}$	$7.11\cdot10^{-3}$	254	5.1
[Oliveira 2007]	N/A	$1\cdot10^{-14}$	0.05	$3.45\cdot10^{-7}$	$4.52\cdot10^{-13}$	$6.31\cdot10^{-8}$	$7.11\cdot10^{-3}$	0.0038	0.1179
[Montastruc 2002]	N/A	$1.004\cdot10^{-14}$	$5.888\cdot10^{-2}$	$347.536\cdot10^{-9}$	$4.539\cdot10^{-13}$	$6.237\cdot10^{-8}$	$7.129\cdot10^{-3}$	$1.824\cdot10^{-3}$	$3.91\cdot10^{-2}$
[Koutsoukos 1981]	$2.35\cdot10^{-59}$ (37ºC)	N/A	25.12 (37ºC)	$3.46\cdot10^{6}$ (37ºC)	$2.33\cdot10^{12}$ (37ºC)	$1.46\cdot10^{7}$ (37ºC)	$1.7\cdot10^{2}$ (37ºC)	$6.81\cdot10^{2}$ (37ºC)	31.9
[Vereecke 1990]	$7.94\cdot10^{-15}$	$1.02\cdot10^{-14}$	$1.73\cdot10^{-13}$	$7.94\cdot10^{-14}$	$6.06\cdot10^{-20}$	$6.31\cdot10^{-8}$	141.25	25.7	$1.58\cdot10^{5}$
[Recillas 2012]	$1.69\cdot10^{-53}$‖ $4.79\cdot10^{-59}$	$1\cdot10^{-14}$	32.4	$2.9\cdot10^{6}$	$2.33\cdot10^{12}$	$1.58\cdot10^{7}$	164.1	681	31.91

	(25°C || 37°C)								
[Attia 1988]	N/A	N/A	23.4423	$2.88 \cdot 10^{6}$	$1 \cdot 10^{-12}$	$1 \cdot 10^{-7}$	$6.31 \cdot 10^{-3}$	512.861	12.023
[Xiong Lu 2005]	$2.35 \cdot 10^{-59}$	N/A	25.12	$3.46 \cdot 10^{6}$	$6.46 \cdot 10^{-13}$	$6.53 \cdot 10^{-8}$	$6.37 \cdot 10^{-3}$	$6.81 \cdot 10^{6}$	$6.81 \cdot 10^{2}$
[Tung 1988]	N/A (25°C || 37°C)	$1.013 \cdot 10^{-14}$ || $2.41 \cdot 10^{-14}$ (25°C||37° C)	20||20 (25°C||37° C)	$2.9 \cdot 10^{6}$||$2.9 \cdot 10^{6}$ (25°C || 37°C)	$4.52 \cdot 10^{-13}$||$6.84 \cdot 10^{-13}$ (25°C||37° C)	$6.31 \cdot 10^{-8}$||$6.58 \cdot 10^{-8}$ (25°C||37° C)	$7.11 \cdot 10^{-3}$||$6.22 \cdot 10^{-3}$ (25°C||37° C)	264||355 (25°C || 37°C)	8.48||7.01 (25°C||37 °C)
[Feenstra 1979]	N/A	N/A	20	$2.9 \cdot 10^{6}$	$4.3 \cdot 10^{-13}$	$6.339 \cdot 10^{-8}$	$7.11 \cdot 10^{-3}$	548	25.6

*Where K is given at temperature values of 25°C, unless otherwise stated

Appendix C. Numerical analysis/Algorithm Logic for the Updated Mathematical Model

Part A: Aqueous Phase Reactions

The first step was to model the aqueous phase without precipitation at equilibrium. The reactions and their equilibrium constants are taken from Table 6 and 7, respectively. The nonlinear system of equations has 11 unknowns and 11 equations (eight aqueous reactions and three mass balances) to solve through. The pH of the system is left as a degree of freedom, allowing the concentration of H^+ to be changed within the model. The equilibrium values of each species are then determined.

Part B: Biology of Mineralization

The biological component of mineralization consisted of five ordinary differential equations. Osteoblasts secrete an organic bone matrix, which begins in its naïve state and is processed by collagen crosslinking and cleavage of C- and N-terminal propeptides from the collagen molecule in order to mature the organic matrix, constituting the first two equations. To prevent naïve matrix from mineralizing, inhibitors are present in the extracellular environment for the third equation. Nucleators are required to initialize mineral precipitation and are removed in proportion to the amount of mineral formed, constituting the fourth equation. Lastly, mineral dynamics were found to be similar to the Hill-type functions and are subsequently expressed in the fifth equation. These are solved using the stiff ode15s solver in MatLab, as differential

algebraic equations are being used in this particular model. The results for each parameter were plotted.

Part C: Biology Integrated with Aqueous Phase of Mineralization for Mineral Formation

The equilibrium values of each species are determined for equilibrium with precipitation of HaP present. Equilibrium values of each species are determined and are used in equation (3c) as the initial concentration being subtracted from the solubility product of HaP. The mineral growth is iterated for the amount of days (120 days in this case), updating the mineral total with respect to the availability of ions present due to the volume constraint introduced. The mineral total (as a function of max mineralization) is then integrated in equation (4a) to produce the combined biological and physicochemical effects. The resulting outcome and values are then displayed.

Appendix D. MATLAB Source Code

```
%%%%%%%%%%%%%%%%%%% PART A - Aqueous Phase Reactions %%%%%%%%%%%%%%%%%%%%%%%%
%%%%%%%                                                                 %%%%%%%
%%%%%%%%%%%%%%%%%%%%%%%%%%%%%%%%%%%%%%%%%%%%%%%%%%%%%%%%%%%%%%%%%%%%%%%%%%%

function F = EquilibriumApproach (x)

%Equilibrium Constant (K) Values
KOH = 1.01*10^-14;
KCaOH = 20;
KHPO4 = 4.05*10^-13;
KH2PO4 = 3.52*10^-8;
KH3PO4 = 7.11*10^-3;
KCaHPO4 = 254;
KCaH2PO4 = 5.1;
KCaPO4 = 2.88*10^6;

MCaT = 1.21*10^-3;
MPO4T = 1.28*10^-3;
MHT = 41*10^-9;

%x1: OH, x2: H, x3: Ca, x4: CaOH, x5: PO4, x6: HPO4, x7: H2PO4, x8: H3PO4,
%x9: CaHPO4, x10: CaH2PO4, x11: CaPO4

eq1 = (KOH*(0.903*x(2))^(-1))-(0.903*x(1));
eq2 = (KCaOH*(0.665*x(3))*(0.903*x(2))^(-1))-0.903*x(4);
eq3 = (KHPO4*(0.399*x(5))*(0.903*x(2)))-0.665*x(6);
eq4 = (KH2PO4*(0.399*x(5))*(0.903*x(2))^2)-0.903*x(7);
eq5 = (KH3PO4*(0.399*x(5))*(0.903*x(2))^3)-1*x(8);
eq6 = (KCaHPO4*(0.665*x(3))*(0.399*x(5))*(0.903*x(2)))-1*x(9);
eq7 = (KCaH2PO4*(0.665*x(3))*(0.399*x(5))*(0.903*x(2))^2)-0.903*x(10);
eq8 = (KCaPO4*(0.665*x(3))*(0.399*x(5)))-0.903*x(11);
eq9 = x(3)+x(4)+x(9)+x(10)+x(11)-MCaT;
```

```
eq10 = x(5)+x(6)+x(7)+x(8)+x(9)+x(10)+x(11)-MPO4T;
eq11 = x(2)+x(6)+2*x(7)+3*x(8)+x(9)+2*x(10)-x(1)-x(4)-MHT;

F = [eq1;eq2;eq3;eq4;eq5;eq6;eq7;eq8; eq9; eq10; eq11];

end

%%%%%%%%%%%%%% Enter in Command Line to display ONLY Aqueous Phase %%%%%%%%
%%%%%%%%%%%%%%%%%%%%%%%%%%%%%%%%%%%%%%%%%%%%%%%%%%%%%%%%%%%%%%%%%%%%%%%%%%%

% options = optimoptions('fsolve','Display','iter'); %displays iterations
needed to solve for equilibrium state at initial conditions
% options.MaxIter = 50000000;
% options.MaxFunEvals = 20000000;
% x0 = [1,1,1,1,1,1,1,1,1,1,1]; %Initial Guesses
%
%for d = 0:1:250
% [x,fval] = fsolve(@EquilibriumApproach,x0,options) %Solver outputting array
with 11 values in "x"
%
% Ksp = 2.35*10^-59; %Solubility Product of Hydroxyapatite
%
% Saturation =
(((x(3)^5)*0.665*(x(1))*0.903*(x(5)^3)*0.399)/Ksp)^(1/9); %Saturation state
calculations
%
% I = x(1)+x(2)+4*x(3)+x(4)+4*x(6)+9*x(5)+x(7)+x(10)+x(11); %Sum of charged
elements to determine the ionic strength of the solution
%

% subplot(3,4,1); %43%    %Subplot each specie here from x(1) to x(11)
% plot(MCaT, x(1),'b.-');
% xlabel('MCaT(mM)');
% ylabel('OH Concentration (mM)');

%MCaT = MCaT+0.00001*q; %Increase MCaT when plotting MCaT vs species

%end


%%%%%%%%%%%%%%%%%%% PART B - Biology of Mineralization ONLY %%%%%%%%%%%%%%%%
%%%%%%%  Program to solve system of ordinary differential equations %%%%%%%
%%%%%%%%%%%%%%%%%%%%%%%% modelling bone mineralization %%%%%%%%%%%%%%%%%%%%%%

function BiologyMineralizationOnly()
 % Nondimensionalized parameter values:
 % Fixed Values

 k1 = 0.1; % Inversely related to time lag and max mineralization
 % (Decreasing k1 by a factor of 3 increases time lag
 % to 40 days.)

 k2 = 1; % This value is fixed.

 k3 = 1; % Directly related to max mineralization.
```

```
v1 = 0.1; % Directly affects max I, and inversely affects time-
% lag in some range of values of r1.

% Values fit to healthy model
r1 = 0.2; % Affects time lag (inversely) & mineralization
% (directly)
r2 = 17; % Affects mineralization (inversely) - intrafibrillar rate
%r2inter = 17; %interfibrillar rate
a = 10;
b = 0.001; %


% Calculation of physical parameter values from
% nomdimensionalized parameter values
xhat = 1e6;
yhat = 1e9;
k1_physical = k1;
v1_physical = v1;
r1_physical = r1/xhat;
k2_physical = k2;
k3_physical = k3*yhat/xhat;
r2_physical = r2/(k3_physical*xhat);


fprintf('PARAMETERS: Nondimensional Physical \n');
fprintf('-----------------------------------------\n');
fprintf(' k1: %13e %13e\n',k1,k1_physical);
fprintf(' k2: %13e %13e\n',k2,k2_physical);
fprintf(' k3: %13e %13e\n',k3,k3_physical);
fprintf(' r1: %13e %13e\n',r1,r1_physical);
fprintf(' r2: %13e %13e\n',r2,r2_physical);
fprintf(' v1: %13e %13e\n',v1,v1_physical);


function Zdot = rhs(t,z) %z=(x1,x2,I,N,y)
Zdot=zeros(5,1);
Zdot(1) = -k1*z(1); %Naive Collagen Matrix
Zdot(2) = k1*z(1); %Mature Collagen Matrix Formation
Zdot(3) = v1*z(1) - r1*z(2)*z(3); %Inhibitors
Zdot(4) = k2*k1*z(1) - r2*H(z(3))*z(4)*z(4); %Nucleators
Zdot(5) = k3*H(z(3))*(z(4)); %Mineral formation
end

function hill = H(x)
hill = b/(b+x^a);
end

% Implement built in ODE solver
% t0, t1 X1,X2,I, N, N2, Y1, Y2, Y3
 [T,Y] = ode15s(@rhs, [0, 120], [1, 0, 1, 0, 0]);
```

```
 Imax = ceil (max( Y(:,3) ) );
 plot(T,Y(:,1),'c:', 'LineWidth',2) ;hold on
 plot(T,Y(:,2),'g-.', 'LineWidth',2) ;hold on
 plot(T,Y(:,3)/Imax,'r:','LineWidth',2) ;hold on
 plot(T,Y(:,4),'y-', 'LineWidth',2) ;hold on
 plot(T,Y(:,5),'b-', 'LineWidth',2) ;hold on

 strI = strcat('I/',sprintf('%d: Inhibitor/Max',Imax));
 legend('X_1: Collagen','X_2: Crosslinked',strI,...
 'N: Inter/Intra Nucleator', 'Y(Ha): HA Mineral', ...
'Location', 'SouthEast');

 axis( [0,120,0,1.2] )
 xlabel('Time in days')
 ylabel('Concentration')
 title('Bone Minealization')

 end

%%%%%%%%%%%%%%%%%% PART C - Physicochemistry and Biology %%%%%%%%%%%%%%%%%%%%
%%%%%%%  Program to solve system of ordinary differential equations %%%%%%%
%%%%%%%%%%%%%%%%%%%%%%%% modelling bone mineralization %%%%%%%%%%%%%%%%%%%%%%

function BoneMineralization ()

k1 = 0.1; % Inversely related to time lag and max mineralization
 % (Decreasing k1 by a factor of 3 increases time lag
 % to 40 days.)

 k2 = 1; % This value is fixed. Currently the addition of kintra+kinter to
get the constant value

 v1 = 0.1; % Directly affects max I, and inversely affects time-
 % lag in some range of values of r1.

 % Values fit to healthy model
 r1 = 0.2; % Affects time lag (inversely) & mineralization
 % (directly)
 r2 = 17; % Affects mineralization (inversely) - intrafibrillar rate
 %r2inter = 17; %interfibrillar rate
 a = 10;
 b = 0.001; %


 % Calculation of physical parameter values from
 % nomdimensionalized parameter values
 xhat = 1e6;
 k1_physical = k1;
 v1_physical = v1;
 r1_physical = r1/xhat;
 k2_physical = k2;
 k3_physical = 1e-3;
 r2_physical = r2/(k3_physical*xhat);
```

```
 fprintf('PARAMETERS: Nondimensional Physical \n');
 fprintf('-----------------------------------------\n');
 fprintf(' k1: %13e %13e\n',k1,k1_physical);
 fprintf(' k2: %13e %13e\n',k2,k2_physical);
 fprintf(' r1: %13e %13e\n',r1,r1_physical);
 fprintf(' r2: %13e %13e\n',r2,r2_physical);
 fprintf(' v1: %13e %13e\n',v1,v1_physical);


MCaT = 1.21*10^-3;
MPO4T = 1.28*10^-3;
MHT = 41*10^-9;

V = 1*10^-12;    %1*10^-18 m3 is 1 um3, units in meters

function F = EquilibriumApproach(x)

KOH = 1.01*10^-14;
KCaOH = 20;
KHPO4 = 4.05*10^-13;
KH2PO4 = 3.52*10^-8;
KH3PO4 = 7.11*10^-3;
KCaHPO4 = 254;
KCaH2PO4 = 5.1;
KCaPO4 = 2.88*10^6;

%x1: OH, x2: H, x3: Ca, x4: CaOH, x5: PO4, x6: HPO4, x7: H2PO4, x8: H3PO4,
%x9: CaHPO4, x10: CaH2PO4, x11: CaPO4

eq1 = (KOH*(0.903*x(2))^(-1))-(0.903*x(1));
eq2 = (KCaOH*(0.665*x(3))*(0.903*x(2))^(-1))-0.903*x(4);
eq3 = (KHPO4*(0.399*x(5))*(0.903*x(2)))-0.665*x(6);
eq4 = (KH2PO4*(0.399*x(5))*(0.903*x(2))^2)-0.903*x(7);
eq5 = (KH3PO4*(0.399*x(5))*(0.903*x(2))^3)-1*x(8);
eq6 = (KCaHPO4*(0.665*x(3))*(0.399*x(5))*(0.903*x(2)))-1*x(9);
eq7 = (KCaH2PO4*(0.665*x(3))*(0.399*x(5))*(0.903*x(2))^2)-0.903*x(10);
eq8 = (KCaPO4*(0.665*x(3))*(0.399*x(5)))-0.903*x(11);
eq9 = x(3)+x(4)+x(9)+x(10)+x(11)-MCaT;
eq10 = x(5)+x(6)+x(7)+x(8)+x(9)+x(10)+x(11)-MPO4T;
eq11 = x(2)+x(6)+2*x(7)+3*x(8)+x(9)+2*x(10)-x(1)-x(4)-MHT;

F = [eq1;eq2;eq3;eq4;eq5;eq6;eq7;eq8; eq9; eq10; eq11];


end

options = optimoptions('fsolve','Display','iter'); %displays iterations
needed to solve for equilibrium state at initial conditions
options.MaxIter = 50000000;
options.MaxFunEvals = 20000000;
x0 = [1,1,1,1,1,1,1,1,1,1,1]; %Initial Guesses

Mineral(1,1) = 0; %At first iteration, no mineral is formed
```

```
count = 120;  %120 days of Mineral formation%

d = 1; %Intitalizing value for array counter for Mineral value, 1 because
MatLab does not recognize array at spot "0"

MolarValueCa = 40.08;  %Molar Mass values for Ca, PO4, and H
MolarValuePO4 = 94.971;
MolarValueH = 1.008;

K = 7*10^15;   %K value

  for c = 2:count %Iterative loop to update the mineral total each day

      [x,fval] = fsolve(@EquilibriumApproach,x0,options) %Solve for x(1) to
x(11) specie concentrations

d = d+1; %Counter for Mineral Array

Ksp = 2.35*10^-59; %Solubility Constant of Hydroxyapatite
n = 3; %Nucleation-type constant

S = (((x(3)^5)*(x(1))*(x(5)^3))/(Ksp))^(1/9); %Supersaturation value

    if S >= 1

    Mineral(1,d) = (1*((x(3)^5*x(5)^3*x(1)^1)^(1/9)-
(Ksp)^(1/9))^n*c)+Mineral(1,d-1); %Mineral formation, which considers the
previous

    TamountMCaT = MCaT*MolarValueCa*V;   %Converted concentrations in amounts
(g)
    TamountMPO4T = MPO4T*MolarValuePO4*V;
    TamountMHT = MHT*MolarValueH*V;

    TnewamountMCaT = TamountMCaT - (5/9)*Mineral(1,d);  %Specie mass (in
grams) is subtracted from mass formed respective to the stochiometric
constants of HaP
    TnewamountMPO4T = TamountMPO4T - (3/9)*Mineral(1,d);
    TnewamountMHT = TamountMHT - (1/9)*Mineral(1,d);

    MCaT = TnewamountMCaT*(1/MolarValueCa)*(1/V);  %New concentrations are
updated by converting mass back to concentration (in mM)
    MPO4T = TnewamountMPO4T*(1/MolarValuePO4)*(1/V);
    MHT = TnewamountMHT*(1/MolarValueH)*(1/V);

    SimMineral = Mineral*K; %K value that increases the value of mineral
formed (in grams)

    end

    if S < 1  %If the Saturation is not greater than 1, Mineral stays the
same as the previous iteration
    Mineral(d) = Mineral(d-1);
    SimMineral = Mineral*K;
```

```
    end

  end

function Zdot = rhs(t,z) %z=(x1,x2,I,N,y)
 Zdot=zeros(5,1);
 Zdot(1) = -k1*z(1); %Naive Collagen Matrix
 Zdot(2) = k1*z(1); %Mature Collagen Matrix Formation
 Zdot(3) = v1*z(1) - r1*z(2)*z(3); %Inhibitors
 Zdot(4) = k2*k1*z(1) - r2*SimMineral(1,rr)*H(z(3))*(z(4))*z(4); %Nucleators
 Zdot(5) = SimMineral(1,rr)*H(z(3))*(z(4)); %Mineral formation with
physicochemitry included

end

 function hill = H(x)      %H(x) changed to P(x)
 hill = b/(b+x^a);
 end

% % Implement built in ODE solver
% % t0, t1 X1,X2,I, N, N2, Y1, Y2, Y3

for rr = 1:120  %counter to move the mineral amount to the next array spot,
each time the ODE solver runs
 [T,Y] = ode15s(@rhs, [0, 120], [1, 0, 1, 0, 0]);
end

 Imax = ceil (max( Y(:,3) ) );
 plot(T,Y(:,1),'c:', 'LineWidth',2) ;hold on
 plot(T,Y(:,2),'g-.', 'LineWidth',2) ;hold on
 plot(T,Y(:,3)/Imax,'r:','LineWidth',2) ;hold on
 plot(T,Y(:,4),'y-', 'LineWidth',2) ;hold on
 plot(T,Y(:,5),'k-', 'LineWidth',2) ;hold on

 strI = strcat('I/',sprintf('%d: Inhibitor/Max',Imax));
 legend('X_1: Collagen','X_2: Crosslinked',strI,...
 'N: Inter/Intra Nucleator','Y(Ha): HA Mineral',...
'Location', 'SouthEast');

 axis( [0,120, 0, 1.2] )
 xlabel('Time in days')
 ylabel('Concentration')
 title('Healthy Bone Mineralization')
 end
```